Chapter 21

Photophosphorylation

Wolfgang Junge

Table of Contents

Abstract

Adenosine triphosphate (ATP), the general fuel of the cell, is the primary product of photosynthesis in most bacteria, and it is one major product, accounting for about 20% of the captured light energy, in oxygenic photosynthesis by cyanobacteria and plants. The proton driven ATP synthase is a paradigmatic enzyme that has it all, an electrical rotary motor being coupled to a rotary chemical generator by a mechanical power transmission. The simplicity and robustness of its construction is just splendid. This chapter describes the interplay of proton pumps and the ATP synthase in photosynthetic organisms and the structure and function of this remarkable enzyme in bacteria and eukarya.

21.1 Introduction

Nature uses adenosine triphosphate (ATP, see Figure 1) as the common fuel to drive chemical syntheses, transport, information processing and other activities of the cell. The (pseudo-)standard molar free energy of ATP hydrolysis is $\Delta G^{\circ}_{\mathrm{ATP}\rightarrow\mathrm{ADP}} = -30\,\mathrm{kJ\,mol^{-1}}$. Its single-molecule mechanical equivalent, $-50\,\mathrm{pN\,nm}$, which equals $-12k_{\mathrm{B}}T$, expresses the fact that ATP hydrolysis provides the necessary driving force to win over chaotic thermal impact, whose energy input is related to the product of the Boltzmann factor (k_{B}) and the temperature (T/K).

ATP is regenerated from adenosine diphosphate (ADP) and (*i*norganic) phosphate (P_i) by photosynthesis (photophosphorylation) and respiration (oxidative phosphorylation). Although the total content of ATP and ADP in an organism is small, the daily turnover can be large. Some ten grams contained in the human body are cycled around to the daily equivalent of the bodyweight.

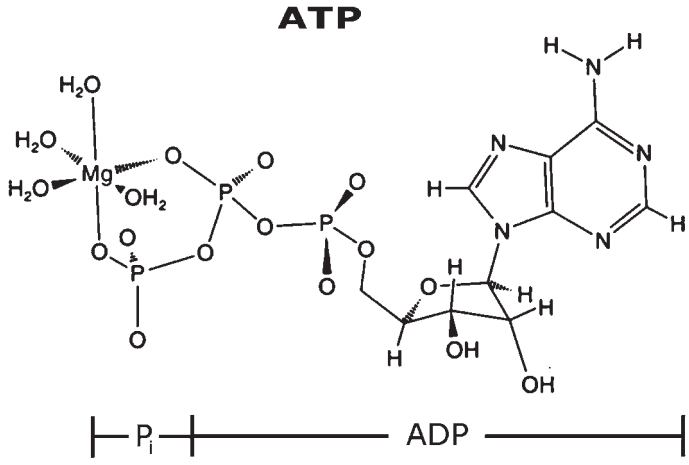

Figure 1. Magnesium adenosine 5′-triphosphate, Mg-ATP.

In purple bacteria ATP-formation accounts for 100% of the useful work recovered from sunlight and in green plants still for 20%.

Fritz Lipmann had already emphasized the universal role of ATP in cellular metabolism in 1941. In 1954 Dan Arnon discovered the production of ATP upon illumination of broken chloroplasts [1]. At that time it was assumed that photosynthetic or oxidative electron transport generated a phosphorylated chemical intermediate followed by phosphoryl-transfer to ADP [2], a mechanism coined substrate level phosphorylation. During the ongoing but futile search for the supposed phosphorylated intermediate Peter Mitchell stirred up the research community when he claimed, in 1961, that ATP might be formed without such an intermediate. Instead, he envisaged the direct coupling of ATP synthesis to proton flow as driven by the transmembrane difference of the electrochemical potential, which he coined protonmotive force [3,4]. He named this hypothesis "chemiosmotic". It became evident that chloroplasts can use an artificially induced pH difference to produce ATP [5], and/or a light induced voltage difference [6]. The bacteriorhodopsin-driven proton pump from *H. halobium* was co-reconstituted in liposomes with the mitochondrial ATP synthase, and they were shown to be functionally coupled by protonmotive force [7]. Ion-driven ATP synthesis and its reversal, ion-pumping under ATP hydrolysis, are now well established in archaea, bacteria and in chloroplasts and mitochondria of eukarya.

The molecular details of the coupling mechanism were not touched upon by Mitchell's hypothesis. The discovery in 1960 of an ATP synthase in mitochondria and the isolation of its soluble portion, the "coupling *f*actor" (F_1), acting on a membrane-embedded portion (now known as F_0) by Ephraim Racker and his co-workers [8] started the search for a molecular mechanism. Three decades after Mitchell's first proposal, the joint attack by protein chemistry, molecular biology, structural biology and biophysics has disclosed the astounding fact that proton flow across the enzyme is *mechanically* coupled to ATP synthesis.

Around 1990 it was established that ATP hydrolysis occurred in alternation between at least two equivalent reaction sites on F_1 by what Paul Boyer coined the "binding change mechanism" [9]. A rotary mechanism, involving three catalytic sites, was considered as a possibility [10] (see [11] for review). The crystal structure of bovine mitochondrial F_1, elucidated by John Walker and his colleagues [12], suggested that rotation, and not alternation, was nature's choice (see [13] for a review). The structure revealed six nucleotide binding sites falling into two classes that are now understood as catalytic and non-catalytic – their position alternates in the hexagon of $(\alpha\beta)_3$. In the crystal structure the former three were differently filled, being empty, containing ADP, and AMP-PNP (as ATP analogue). This was interpreted as a still picture of three, in principle, equivalent catalytic sites that, when driven by the rotation of the central stalk, change their role, one binding ADP and P, the next processing it into ATP and third releasing ATP and so on, cyclically. A rotary mechanism is supported by a biochemical assay using cleavable crosslinks [14]. It was time resolved by polarized laser-photometry [15], and spectacularly proven by

Hiruyuki Noji in the laboratories of Masasuke Yoshida and Kazuhiko Kinosita, who applied a fluorescent actin-filament to the rotor portion of the immobilized enzyme and videographed the rotation [16].

The present view of the ATP synthase is that of a molecular twin machine. The catalytic function is contained in the soluble portion (F_1) and the ion-transporting function in the membrane-intrinsic portion (F_0), each being a rotary motor/generator. They are coupled by a central rotary shaft and held together by an eccentric stalk (Figure 2B). Figure 2(B) also accounts for the fact that there are crystal structures on certain portions of the enzyme and less detailed information on others.

This chapter starts with an up-to-date view of the tenets of the chemiosmotic theory, covers proton pumps and pathways, the proton-to-ATP stoichiometry and the enzyme regulation in a physiological context. Up to this point it is focused on photosynthetic organisms. The subsequent description of ATP synthase as a rotary electro-mechano-chemical transducer merges knowledge obtained with this enzyme from different kingdoms of life. This accounts for the fact that the enzyme emerged before the separation of archaea and eubacteria, and that it has been conserved to an astounding similarity over the former and in chloroplasts and mitochondria of eukarya.

Usually, the terms F-ATPase, F_0F_1-ATPase, and ATP synthase are used synonymously. The proton driven, membrane-intrinsic portion is termed F_0 (for historical reasons the suffix reads capital O, not zero) and the peripheral portion that performs ATP synthesis/hydrolysis is termed F_1. Where species specific properties are discussed, the letters C for *c*hloroplast, M for *m*itochondrion, B for purple *b*acterium, E for *E. coli*, T for the *t*hermophilic *Bacillus PS3*, P for the Na^+-translocating *P. modestum*, and A for *a*rchaeon annexed to the F. Thus, CF_0F_1 denotes the ATP synthase of chloroplasts.

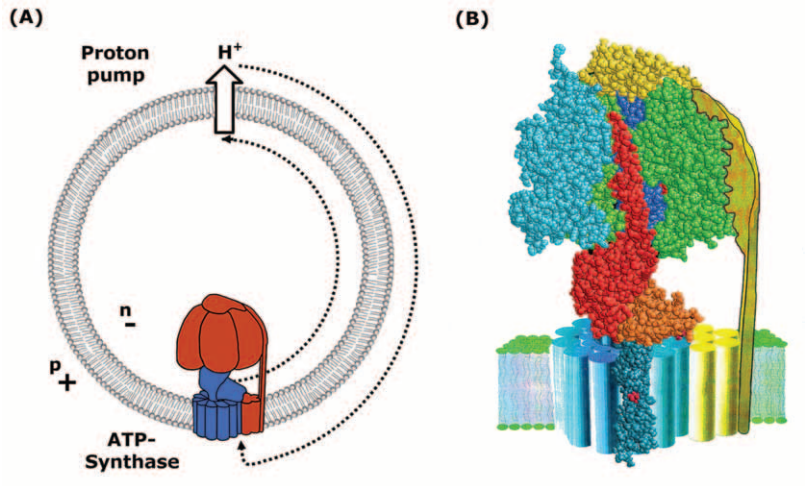

Figure 2. (A) Chemiosmotic mechanism of ATP synthesis. (B) ATP synthase.

21.2 Chemiosmotic Energy Coupling

The synthesis/hydrolysis of ATP proceeds according to the following reaction scheme (written for aqueous medium at pH 8, for stability constants see [17]):

$$ADP^{3-} + P_i^{2-} + H^+ \leftrightarrow ATP^{4-} + H_2O \quad (1)$$

Before 1960 it was assumed that photosynthetic or respiratory electron transfer was directly linked to ATP synthesis. Bob Williams introduced a new twist by emphasizing a role for the proton [18,19]. He thought of electron transport generating an extreme acidic milieu ''inside the membrane'' to shift the equilibrium [eqn. (1)] towards ATP. Taken at face value (ADP, P_i and ATP had to be moved into and out of the membrane!) this view had obvious flaws right from the beginning, but in milder form ''membrane localized'' protons have remained around for quite a while. At the same time Peter Mitchell also emphasized the role of protons, but he took the membrane simply as a permeability barrier between two aqueous phases and postulated two now well-established properties of the membrane: (i) zig-zagging vectorial electron/hydrogen transfer, generating a difference of the electrochemical potential of the proton between the aqueous phases, and (ii) the ATP synthase utilizing the ''protonmotive force'' by transporting protons from the acid and electropositive side to the alkaline and negative one [3,4]. It implied adding of m ''vectorial protons'' to the one ''scalar proton'' in eqn. (1).

$$ADP^{3-}_n + Pi^{2-}_n + H^+_n + mH^+_p \leftrightarrow ATP^{4-}_n + H_2O + mH^+_n \quad (2)$$

Herein m denotes the number of protons that are transported from the positive (p) side to the negative (n) side of the membrane for every ATP molecule that is formed at the n-side. The scalar proton ($H^+{}_n$) accounts for electroneutrality if the ionization states of the nucleotides and of phosphate are as given in eqn. (1) (written for pH 8). Broadly speaking, Mitchell's concept, as simplified in Figure 2(A) has been validated, except for refinements, as given in Section 21.2.3.

21.2.1 Energetics

The basic tenets of the chemiosmotic hypothesis are proton pumps, which generate a difference of the electrochemical potential across the coupling membrane, and the ATP synthase, which couples the backflow of protons to ATP synthesis (Figure 2A). The electrochemical potential difference of the proton, in Mitchell's term the ''protonmotive force'' (p.m.f.), is given by:

$$\text{p.m.f.} = \Delta\mu^0 - 2.3\,RT\Delta\text{pH} + F\Delta\varphi$$

If the aqueous phases have the same properties (their standard potentials being equal, $\Delta\mu^0 = 0$) it reduces to:

$$\text{p.m.f.} = -2.3\,RT\Delta\text{pH} + F\Delta\varphi \quad (3)$$

wherein ΔpH and $\Delta\varphi$ denote the transmembrane pH difference (pH_n–pH_p) and the electric potential difference (ϕ_n–φ_p in volt), T is the temperature (in Kelvin), R is the universal gas-constant and F the Faraday constant. Under isothermal and isobaric conditions the p.m.f. describes the maximum useful work that can be derived from the translocation across the membrane of one mol proton. It is equivalent to the molar Gibbs Free Energy difference, $\Delta\overline{G_{H^+}}$. The often used term "proton gradient", a lab slang, should be avoided, neither has the proton any gradient nor does the local first derivative matter in this context. The equivalence of the electrical and the chemical contribution to the p.m.f. in determining the production of ATP holds only for the thermodynamic equilibrium, i.e., for processes conducted at infinitely slow speed. Far from the equilibrium, a physiologically more relevant regime, it is probably violated [20].

At 25°C or 298.15 K the numerical factors are $2.3RT = 5.7\,\mathrm{kJ\,mol^{-1}}$, and $2.3RT/F = 59\,\mathrm{mV}$, so that eqn. (3) accounts for the fact that a voltage of –59 mV contributes as much to the driving force as a pH difference of +1 unit. In single-molecule terms these figures are often given in pN nm ("pico-Newton-nanometer") or in units of k_BT, with $5.7\,\mathrm{kJ\,mol^{-1}}$ being equivalent to 9.5 pN nm or $2.3\ k_BT_{298.15}$.

In reality, the aqueous phases at both sides of a coupling membrane differ. Not only are the membrane surfaces covered with fixed charges but the often narrow "bulk phases" are differently filled with proteins, i.e., polyelectrolytes. These complications invoke surface- and Donnan-potentials. Both are equilibrium potentials, i.e., the electrochemical potential of the proton at the surface equals that in an adjacent bulk phase (if there is any bulk), but the distribution of energy between the electric ($\Delta\varphi$) and the chemical component (ΔpH) differs.

Peter Mitchell postulated that the strict coupling of ATP synthesis with the transfer of m protons gives rise to the net reaction in eqn. (2). A cell synthesizing ATP at higher velocity than it is consumed will eventually reach the "static head" where the forward and the backward reaction compensate each other. If the consumers of ATP in the cytoplasm and those of p.m.f. in the membrane are slow enough this state approximates the equilibrium, such that the p.m.f. is balanced by the molar free energy of ATP hydrolysis:

$$m \times \text{p.m.f.} = \Delta G^0_{\mathrm{ATP}\rightarrow\mathrm{ADP}} + 2.3RT \log \frac{[\mathrm{ADP}][\mathrm{P_i}][\mathrm{H^+}]}{[\mathrm{ATP}]} \qquad (4)$$

wherein m denotes the proton-over-ATP stoichiometry (not necessarily an integer, see below), [X] is the dimensionless activity of the respective species X, and RT is as usual. All activities are dimensionless and normalized to 1 M, except for the one of the proton, where normalization is to 10^{-7} M (pH 7). $\Delta G^{\circ}{}_{\mathrm{ATP}\rightarrow\mathrm{ADP}}$, the pseudo-standard free energy of ATP hydrolysis is $-30\,\mathrm{kJ\,mol^{-1}}$ at pH 7, 1 mM Mg^{2+}, and an ionic strength of 0.2 M. For the dependence of $\Delta G^{\circ}{}_{\mathrm{ATP}\rightarrow\mathrm{ADP}}$ on these parameters see [21].

The balance between the stoichiometry-weighted p.m.f. [eqn. (4), left] and the so-called phosphate potential [eqn. (4), right] determines whether ATP is formed or hydrolyzed. In thermodynamic equilibrium they are equal. For

illuminated chloroplasts the following stroma concentrations have been reported: ATP (2.5 mM), ADP (0.5 mM), P_i (5 mM), pH 8. The calculated phosphate potential [eqn. (4), right] is 53 kJ mol^{-1}. If the H^+/ATP-stoichiometry was 4, which is debatable (Section 21.2.4), the p.m.f. sustaining this phosphate potential should amount to 2.3 pH units or 136 mV.

21.2.2 Photosynthetic Membranes

Photosynthesis is of prokaryotic origin and so is ATP synthesis. Figure 3(A, C) illustrates the outer and inner membrane of a purple bacterium, e.g., *Rhodobacter capsulatus*, whose plasma membrane forms invaginations carrying the whole complement for photosynthesis, named chromatophores (see also Chapters 1 and 18). In prokarya, proton pumping is outward directed; the backflow into the cytoplasm drives the synthesis of ATP, which is released into the cytoplasm. The compartment into which protons are pumped is termed p-side (positive side) and the opposite one n-side. If chromatophores are isolated by sonication of bacteria they reseal as inside-out vesicles, so that protons are pumped into their small lumen, and ATP is released into the suspending medium. In the chloroplasts of green plants (Figure 3B and D) these former invaginations are sealed off from the envelope. They form an interlaced

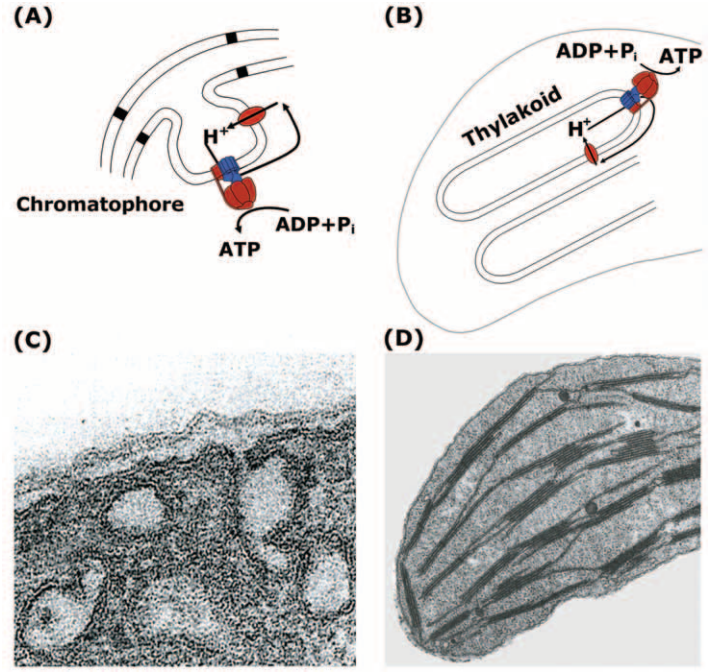

Figure 3. Photosynthetic membranes (schematic): (A, C) Purple bacterium with c chromatophore [120], (B, D) Chloroplast with thylakoids. [Courtesy of Andrew Staehelin.]

network of thylakoid membranes. Protons are pumped into the lumen and ATP is released into the chloroplast stroma. If thylakoids were fused into the outer membrane of chloroplasts the lumen formed part of the peri- or exoplasma of the chloroplast. Thylakoids form a tightly apposed system of disk-shaped membranes (these stacks appearing as "grana" in the light microscope) with a repeat distance of only 20 nm and about 5 nm thin spacing in the outer partitions and in the lumen. The grana are interconnected by "stroma lamellae" (Figure 3C, see also Chapter 1).

The volume of the lumen of one disk is so small that one wonders whether the pH is well defined in such a small compartment. Taking the typical diameter of one disk as 400 nm and a thickness of 5 nm, one calculates a volume of only $6 \times 10^{-22}\,m^3$. At pH 7, a proton concentration of $10^{-4}\,mol\,m^{-3}$, the number of hydrated ("free") protons in this volume is less than 0.05. Contrary to the first impression, the smallness of the volume does not imply that the pH is ill-defined so that it varies greatly from one disk to the other. Instead, protons dissociate from and associate with thousands of buffering groups on proteins and lipids at the lumenal surface of the membrane, each with a typical rate (at pH 7) of $10^4\,s^{-1}$. This implies that the standard deviation from the average proton concentration is very small indeed, such that the mean pH is well defined in the time average at the millisecond time scale where ATP synthesis occurs.

Notably, the complicated web of grana and interconnecting stroma lamellae in one chloroplast forms a very large contiguous sheet. Contiguity has been evident from both structural and functional studies. The osmotic swelling of broken thylakoids produces large blebs of up to 20 μm diameter [22] and EM-pictures have suggested the interlacing of grana [23]. Studies on the electric discharge rate in thylakoids have revealed that a single dimer of the potent ionophore gramicidin accelerates the electric discharge across the membrane patch containing at least 5×10^7 chlorophyll molecules, which is close to the estimated number of 2×10^8 total per chloroplast [24]. This implies that almost all electrogenic pumps can be (at least electrically) coupled with all ATP synthases by one contiguous membrane. The tightly apposed grana lamellae and the exposed stroma lamellae have different lipid and protein composition. Photosystem II (PS II) is enriched in the stacked domains whereas Photosystem I (PSI) and the F_0F_1-ATPase are located in the stroma-exposed regions of the thylakoid membrane (see also Chapter 1). Their segregation by several 100 nm does not bear much on the efficiency of coupling – it is only slightly lower for PS II-driven photophosphorylation than for PSI-driven one.

21.2.3 Proton Pumps and Pathways

Absorption of a quantum of light induces a very rapid charge separation in photosynthetic reaction centers. The vectorial electron transfer from the p- to the n-side electrically charges the coupling membrane in less than one nanosecond ($10^{-9}\,s$). The high speed of voltage generation has been resolved spectrophotometrically by using the molecular voltmeters that are intrinsic to many photosynthetic membranes, namely the electrochromic response of

carotenoids and chlorophylls [25–29]. The magnitude of the rapid voltage jump induced, e.g., by a laser flash of nanosecond duration, ranges from 30 to 50 mV in thylakoids to 70 mV in chromatophores [29,30]. These figures are broadly compatible with structural data on photosynthetic membranes. In plant thylakoids the membrane area per chlorophyll molecule has been estimated to be $2\,nm^2$; there are about 600 chlorophyll molecules per two photosystems, and the specific electric capacitance of biomembranes is usually $10^{-2}\,F\,m^{-2}$.

Vectorial electron transfer causes net proton translocation by alternating with vectorial hydrogen transfer. When Photosystem II of cyanobacteria and plants or the related reaction centre of purple bacteria (BRC) reduce their respective plant quinone, one proton per electron is taken up at the n-side of the membrane. When PS II extracts electrons from water to produce dioxygen it ejects one proton per electron at the p-side. Thereby, PS II is both electrogenic (by primary electron transfer) and (net) proton pumping, the latter as the result of one vectorial and two scalar reactions. The quinol that is formed at the n-side of PS II, and likewise of BRC, acts as a hydrogen carrier when diffusing over to the p-side to reduce cytochrome b_6f in green plants, and cytochrome bc_1 in bacteria (Chapter 20). Upon oxidation of the respective quinol at the p-side one proton per electron is released. The two electrons from the quinol proceed along different pathways. Whereas the first is transferred to plastocyanin (in plants), cytochrome c_6 (in cyanobacteria) and cytochrome c_1 (in purple bacteria), respectively, the second is transported back across the membrane within the protein to eventually reduce quinone at the n-side. This Q-cycle (in P. Mitchell's terms [31]) is again both electrogenic and proton pumping, being linked to proton uptake at the n-side and proton release at the p-side (for details see Chapter 20). Plastocyanin and cytochrome c_6 eventually reduce PSI (in plants and cyanobacteria, respectively), and cytochrome bc_1 reduces BRC (in purple bacteria), and when another quantum of light drives the next rapid charge separation it is again linked to proton uptake at the n-side. In oxygenic photosynthesis the stoichiometry of protons pumped/voltage generated/electrons transferred is 2:2:1 for the linear electron transport chain from water to $NADP^+$ and further on, and it is 3:3:1 including the cyclic operation and extra proton pumping round of the cytochrome bc_1 (b_6f)-complex.

P. Mitchell's concept that all proton pumps are electrochemically coupled with all ATP synthase molecules by the same bulk-to-bulk protonmotive force has been frequently challenged over the years and detailed models for localized coupling were put forward, favoring, for example, neighbor-to-neighbor coupling, or intra-membrane proton conducting domains, or enhanced proton diffusion at the membrane surface (see [32–35] for reviews). The interest in these models has since faded, except when dealing with alkaliphilic bacteria. These organisms live at pH 10, and they reportedly sustain a bulk-to-bulk p.m.f. close to zero. It has been difficult to understand how they can produce ATP by a F_0F_1-type enzyme, if not by a non-Mitchellian mechanism [36]. The dogma of bulk-to-bulk coupling has recently been reevaluated by standard theory of proton diffusion and assuming an "infinite sink" for protons in the p-phase, as encountered by alkaliphilic bacteria at pH 10 [37,38].

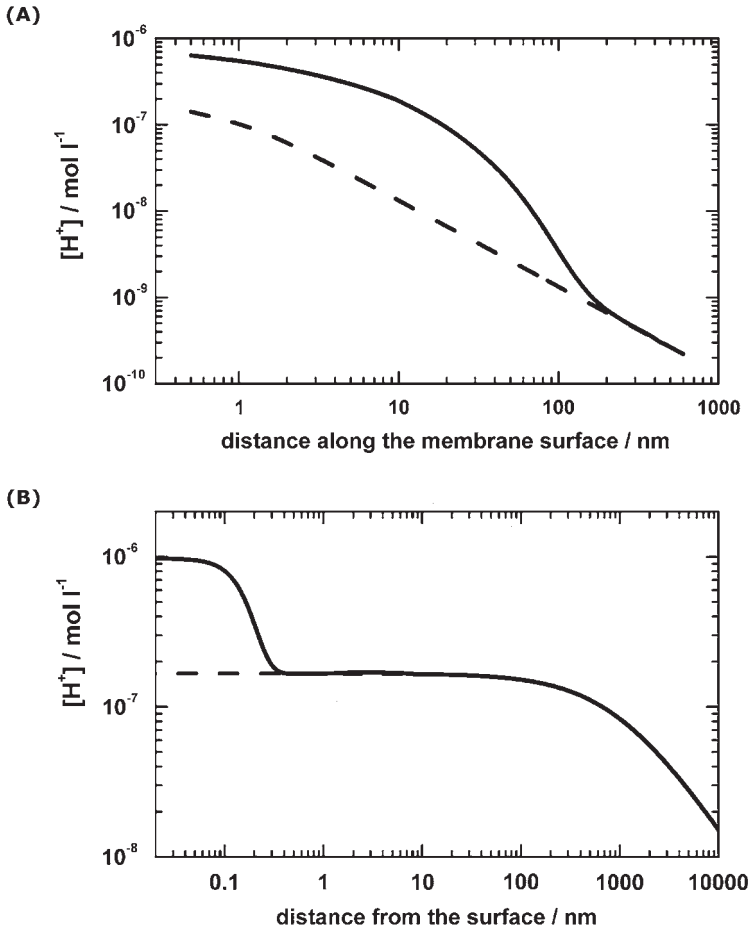

Figure 4. Steady-state pH-profiles at the surface of a proton-ejecting membrane [37]. (A) Proton distribution along a planar membrane containing only one proton pump. The cylindrical axis z is perpendicular to the membrane plane, and the axis r is directed along the membrane. The protons ejected by the pump are spread initially along the membrane surface and then escape through the interfacial barrier (no proton sinks in the membrane were considered). The turnover rate of the pump was $5 \times 10^2\,s^{-1}$, the height of the potential barrier was 0.12 eV, the surface potential was −0.06 V, the bulk diffusion coefficient of protons was $10^{-4}\,cm^2\,s^{-1}$; other details of the model are described in the text. (B) Steady-state pH profile at the surface of sealed membrane vesicles with a radius of 1 mm and surface pump density of $2.3 \times 10^{11}\,cm^{-2}$. The potential barrier as calculated for the ionic strength of 0.1 M (solid line) was used in modeling. The dashed line shows the proton concentration as calculated without potential barrier.

Modeling under reasonable assumptions on turnover rates, the mutual distance between proton pumps and ATP synthase molecules, and on the curvature of the membrane revealed that the protonmotive force is greater in the vicinity of a pump than farther away (Figure 4). This result was obtained

without invoking either of the following special mechanisms: (a) enhanced proton diffusion at the membrane surface and (b) a diffusion barrier for protons between the surface and the bulk phase. It holds for steady turnover of pumps and ATP synthase [37,38]. The proton concentration away from one continuously active singular pump and along the membrane surface facing an infinitely alkaline medium is illustrated in Figure 4(A). The one away from the surface of a pump-covered vesicle into the medium is given in Figure 4(B). The effects are more pronounced if there is a diffusion barrier at the membrane surface (solid lines in Figure 4), for which there is some evidence [38]. In conclusion, the delocalized coupling concept of P. Mitchell is basically correct, but it needs modification in as much as the surface-to-surface p.m.f. that drives the ATP synthase may be greater than the bulk-to-bulk one. This effect is particularly pronounced in alkaliphilic bacteria because they pump protons into an alkaline medium (the "infinite sink") and it is much less so in thylakoids, which pump protons into a finite volume, as has been discussed elsewhere (see [37] and references therein).

21.2.4 H^+/ATP Stoichiometric Ratio

The stoichiometric ratio between proton translocation and ATP synthesis has been extensively studied in photosynthetic membranes using both non-invasive generation of p.m.f. by illumination and an artificial one by mixing techniques (pH-jump, salt-jump). The stoichiometric ratio of H^+/ATP in thylakoid membranes and in proteoliposomes was determined by two different approaches, (i) thermodynamical by recording the equilibrium between the protonmotive force and the phosphate potential [eqn. (4)] and (ii) kinetical, disturbing the equilibrium and recording the ratio of transient proton flow over transient ATP synthesis/hydrolysis. Over the decades, published stoichiometric ratios went up from 2 mol H^+ per mol-ATP to over 3.3 to, eventually, 4, the latter figure being the résumé of extensive work by three groups, H. Strotmann's, B. Rumberg's and H. van Walraven's (see [39] and the references therein). P. Gräber's group determined the same figure, namely 4 ± 0.3, for the reconstituted spinach enzyme in liposomes [40]. This agreed figure has resulted from repeated, very careful studies by both the thermodynamic and the kinetic approach, with the enzyme from spinach and cyanobacteria, and by applying several independent techniques to control the magnitude of the protonmotive force and the amount of ATP synthesized/hydrolyzed. Nevertheless the figure of 4 is not compatible with the structural symmetry of the chloroplast enzyme. The rotary electromotor, F_0, of the chloroplast enzyme shows C_{14}-symmetry, and the chemical reactor, CF_1, C_3-pseudosymmetry. The former was determined by atomic force microscopy of the isolated c-ring of CF_0 [41] and the latter by X-ray crystal structure analysis [42].

With 14 proton binding groups in CF_0 and three chemical reaction sites in CF_1 one expects a H^+/ATP-stoichiometry of 4.67 rather than 4. Imperfect coupling of the enzyme (e.g., proton slip in the enzyme or leakiness of the membrane) and a possible underestimation of the protonmotive force

(e.g., because the surface-to-surface p.m.f. is greater than the determined bulk-to-bulk p.m.f.) were both expected to rather overestimate the stoichiometric ratio. Thus, the discrepancy between the structurally expected figure of 4.7 and the thermodynamically and kinetically determined figure of 4 has remained without a convincing rationale.

21.2.5 Regulation

Enzyme molecules are reversible catalysts. An enzyme is denoted as irreversible to indicate that the proportion of active over inactive enzymes in an ensemble is regulated, e.g., by product inhibition. The ATP synthase is regulated by different techniques and in different extent in different organisms. In *E. coli* the enzyme runs reversibly forward or backward depending on the needs of the cell. If the p.m.f. is high, as under aerobic conditions, the enzyme synthesizes ATP, or, should the respiratory protons pumps run low, as under anaerobic conditions, it operates in the reverse direction, hydrolyzing the ATP provided by glycolysis to generate p.m.f. If the chloroplast ATP synthase had the same reversibility, at night, when the light-driven proton pumps of chloroplasts do not work, it would hydrolyze the ATP generated by mitochondria. This is avoided by both p.m.f.- and thiol-regulation of the chloroplast enzyme. CF_0F_1 is down-regulated (i) if the p.m.f. drops below a certain threshold and (ii) if the electron-transport chain fails to sustain a sufficiently reducing milieu.

Figure 5 illustrates the behavior of the reduced (solid curve) and the oxidized enzyme (broken curve) as a function of the p.m.f. The reduced enzyme synthesizes ATP with a turnover number ranging up to $300\,s^{-1}$ if the protonmotive force exceeds 3.5 pH-units. If the p.m.f. is lowered from say 3.5 pH-units to about 2.8 the rate of ATP hydrolysis equals the one of synthesis, i.e., net ATP production is zero. It makes the compensation point where eqn. (4) is expected to hold. If the p.m.f. is lowered further, net ATP hydrolysis dominates until at even lower p.m.f. the enzyme activity is shut off although its driving force prevails. The oxidized enzyme, on the other hand, stops operation before reaching the thermodynamic compensation point, because its p.m.f. threshold for deactivation is augmented by more than a pH unit.

Thiol-regulation relates the activity of F-ATPase to the reducing power of the linear electron transport chain. It is conferred to the enzyme via ferredoxin/thioredoxin, and involves two closely spaced cysteine residues on subunit γ. These are present in the enzyme from green algae and higher plants, but absent in those of bacteria and mitochondria. If these cysteines are engineered into γ of the cyanobacterium *Synechocystis* they confer redox modulation to the mutant enzyme – so far, however, without any detectable benefit for the cell (see [43] and references therein).

The F-ATPase from all sources is regulated by protonmotive force. At least with CF_0F_1 both components, the transmembrane voltage and the pH difference, can activate the enzyme and they do so in equivalent proportion [eqn. (3)]. Activation might require the binding of more than one proton to the enzyme, it is linked to the release of tightly bound ADP from F_1 (see [44] and references

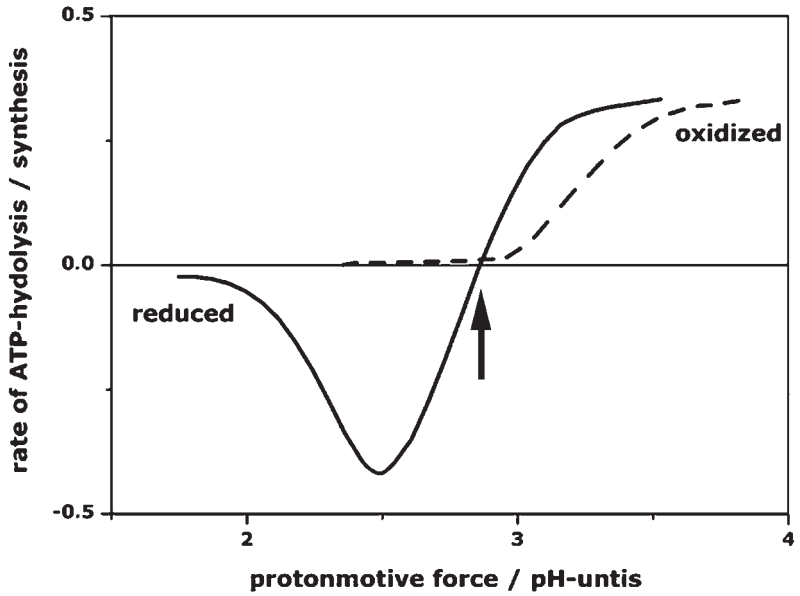

Figure 5. Schematic representation of the p.m.f.- and thiol-regulation of CF_0CF_1 (redrawn after [121]). The rate of net ATP synthesis (positive branch) and hydrolysis (negative branch) as function of the protonmotive force (in pH units), both under oxidizing and reducing conditions. The arrow denotes the thermodynamic compensation point where the phosphate potential is expected to match the protonmotive force according to eqn. (4). The calculated phosphate potential was about 57 kJ mol^{-1} (room temperature) (Figure 2 in [121]). That the calculated compensation point in the respective experiments implies a proton-over-ATP stoichiometry of 3.5 and not 4, as eventually agreed on by several laboratories, or 4.67, as suggested by the enzyme structure (see above), illustrates the difficulties in correctly assessing the p.m.f.

therein), and it involves conformational changes of the ε-subunit. The molecular detail of p.m.f. regulation, with emphasis on the role of subunit ε, is the subject of active research (see [45] and references therein).

A low p.m.f. shuts down both the catalytic activity of F_1 and the coupled proton conductance of F_0 (not the one of exposed F_0, see Section 21.3.3.2). A leak conductance of F_0F_1 is, however, induced at low ADP concentration (<100 nM) and this "proton slip" has been interpreted as a safety valve, protecting the membrane against over-voltage or over-pH-difference. That this is not the case has been demonstrated in chloroplasts where proton slip is blocked by as low as 200 nM of ADP (with mM P_i present) or with 2 μM ATP, conditions that are always met in chloroplasts (see [46] and references therein). Thus, proton slip does probably not function as a safety valve. A similar behavior has been reported for a purple bacterium [47]. Viewed from today, proton slip appears as a consequence of a loose grip of $(\alpha\beta)_3$ on subunit γ if only one out of the three catalytic nucleotide binding sites is occupied. This allows "free" rotation of the rotary proton carrier F_0 (see below).

21.3 ATP Synthase (F_0F_1-ATPase)

21.3.1 Structure

Figure 6(A) illustrates the gross structure of ATP synthase. Its hydrophilic and peripheral portion, F_1, is mounted on the hydrophobic and membrane intrinsic portion, F_0. F_1 and F_0 are held together by a peripheral stalk and a central shaft. The total mass of EF_0F_1 is about 530 kDa and the total height about 20 nm. Soluble F_1 functions as an ATPase, and membrane embedded F_0 without attached F_1 as a proton-conductor. ATP hydrolysis/synthesis by F_1 and proton translocation by F_0 are mechanically coupled. The "rotor" (blue in Figure 6A) rotates against the "stator" portion of the enzyme (brown). The terms stator and rotor are arbitrary, what matters is their relative rotation against each other. The functional rotational turnover time (milliseconds) is longer than the rotational correlation time by diffusion of F_0F_1 (200 μs) [48].

The enzyme's partial functions are attributable to different subunits. For historical reasons the subunit nomenclature differs between organisms – the one for *E. coli* is mostly used in the following. In *E. coli* the composition of the rotor is $\gamma\varepsilon c_{10}$ (molecular masses: 31.4, 14.9 and 8.3 kDa) and the one of the stator $ab_2\delta(\alpha\beta)_3$ (molecular masses: 30.3, 17.2, 19.6, 55.3 and 50.2 kDa). In chloroplasts and in purple bacteria a heterodimer, bb′, substitutes for the homodimer, b_2 [chloroplast nomenclature IV/I/II/$\delta(\alpha\beta)_3$], and in mitochondria there are three subunits in the role of bb′, named b, d and F_6. In *E. coli* all subunits are arranged on a single operon (unc). In chloroplasts the genes are distributed between the plastome and the nuclear genome. The latter codes for three subunits, namely γ, δ and b′ (alias II), and the former for the rest. The hexagon of $(\alpha\beta)_3$ incorporates a total of six nucleotide binding sites. Only three are catalytically active, they are considered in the following. These sites are mainly formed by subunit β at the interface with subunit α.

Four key structural features of F_1 are indicated in Figure 6(B), namely (i) one out of a total of three catalytic nucleotide binding sites on subunit β (in red), (ii) the central curved shaft, subunit γ (in yellow), (iii) the hydrophobic bearing at the N-terminal collar of $(\alpha\beta)_3$ anchoring the C-terminal end of γ, and (iv) the lever on subunit β that is moved back and forth by the rotating "crank"-shaft. These assignments were already made in 1994 when John Walker and collaborators described the first asymmetric crystal-structure of MF_1 [2]. Their function is illustrated in Movie 1. Asymmetric nucleotide occupancy in the three catalytic subunits was apparently required to fix the position of the central shaft in the hexagon of $(\alpha\beta)_3$. Crystal-structures with symmetric occupancy of the nucleotide binding sites have produced lower resolution and, in particular, blurred electron densities in the region of γ [42,49,50]. In the asymmetric crystal structure the convex side of the curved shaft faces the lever on the particular β-subunit with an empty nucleotide binding site. One major feature discriminating between a catalytic site filled with ADP and another one with an ATP-analogue is the redirection of an arginine on subunit α from pointing away from ADP to leaning over to contact the γ-phosphate position of

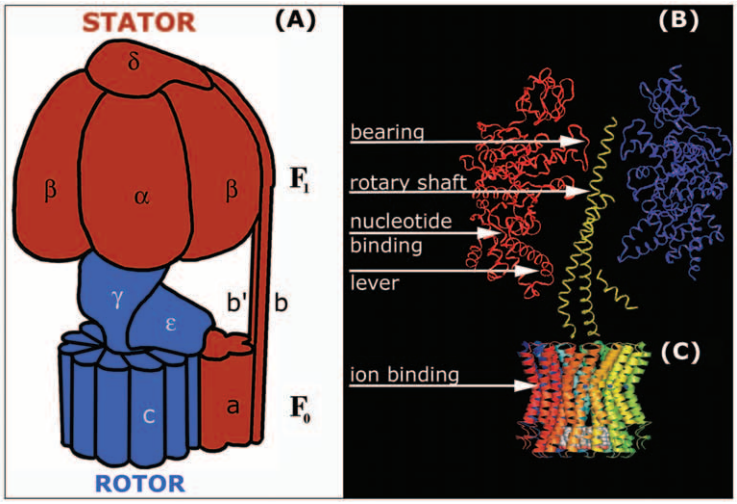

Figure 6. (A) Schematic representation of the ATP synthase from photosynthetic organisms, its subunits, their association with the membrane embedded F_0 and the peripheral F_1, and the bipartite functional units, stator (red) and rotor (blue). (B) A central slab of the F_1 structure [12] (see the interpolative Movie 1[†]) with the mechanical elements of rotary F_1 indicated. (C) Crystal structure of the c-ring of F_0 of the sodium translocating bacterium *Iliobacter tartaricus* [60].

ATP, possibly a fixed but flexible counter-ion to lower the energy penalty of the negatively charged γ-phosphate in the protein.

John Walker and his colleges obtained several different asymmetric crystal structures of MF_1 down to a resolution of 0.2 nm [51]: some with aluminum and beryllium fluorides as planar transition state analogues in the phosphate binding position [51–53], with bound inhibitors [54,55], and a symmetrical structure of $(\alpha\beta)_3$ without nucleotides [56]. Most of the crystal structures published so far showing $(\alpha\beta)_3$ and γ have at least one empty nucleotide binding site, none of them has bound ATP in any site, and the ones with the best resolution have either ADPPNP, $ADP.ALF_3$ or $ADP.(ALF_4)_2$ as ATP analogues bound in one or two sites. It appears as if crystallization selects stable but not necessarily active conformations.

One key element of the rotary electromotor is a ring of identical subunits, subunit c. This subunit, a small hairpin of only 8.3 kDa molecular mass, has been coined "proteolipid" because of its hydrophobicity. Its hairpin folding with an essential acid residue (cArg61 in *E. coli*) located in the middle of the membrane was first revealed by in situ photoaffinity labeling [57], and the homo-oligomeric ring structure by cysteine mapping [58]. Solution NMR of the

[†]Animation of ATP-hydrolysis by F_1 (energy minimized interpolation of the crystal structure) (2001, D. Cherepanov). The movie can be viewed at www.bioligie.uni-osnabrveck.de/biophysik/junge, with permission of Prof. Wolfgang Junge.

isolated c-subunit in a mixed solvent provided a closer look at the structure of the monomer (see [58,59] and references therein), and atomic force microscopy corroborated the ring and led to an assessment of the number of subunits involved (see below). Recently, the crystal structure of the c-ring was elucidated at 0.24 nm resolution. It was obtained from *Ilyobacter tartaricus*, a bacterium with a sodium transporting F_0F_1-ATP synthase [60]. The ring is hour-glass shaped, and composed of eleven identical and hairpin-shaped subunits c (Figure 6C). Each carries one sodium cation, right in the middle of the membrane, that is coordinated by residues from the two legs of one c-subunit plus one residue of a neighboring hairpin. In contrast with the C_{11}-symmetry in *I. tartaricus* the c-ring of the proton translocating yeast enzyme has C_{10}-symmetry (obtained by X-ray crystallography [61]), the one of chloroplasts C_{14}-symmetry (obtained by atomic force microscopy (AFM) [41], the ring of *Spirolina platensis* C_{15}-symmetry (again by AFM) [122], and the ones of *E. coli* and of thermophilic *Bacillus* PS3 C_{10}-symmetry (by crosslinking and function-tests [62,63]). The c-ring of the electromotor of the ATP synthase is, therefore, composed of 10, 11, 14 or 15 identical subunits, depending on the organism. This has the following consequences: (i) The rotary holoenzyme, F_0F_1, copes with symmetry mismatch between F_1 (pseudo-C_3) and F_0 ($C_{10,11,14}$), but it must not (C_{15}). (ii) Different organisms run at a different gear between the electro-chemical and the chemical motor/generator. (iii) The stoichiometric ratio of H^+/ATP is not necessarily an integer number, in chloroplasts it is expected to be 4.67 rather than 4, as has emerged from functional studies (Section 21.2.4). (iv) At equal p.m.f. different organisms can sustain higher or lower ATP/ADP ratios, depending on the respective gear.

In the holoenzyme the c-ring is firmly bound to the rotor elements of F_1, namely the "foot" of subunit γ and subunit ε. This has been evident from the fact that some crosslinks between γ and ε [64], and between ε and c [65], do not inhibit the activity, so that it is reasonable to conceive subunits γ and ε as sitting like a firmly attached spoke on the c-wheel (see [66]).

The subunit **a** of F_0 is likely a transmembrane five-helix bundle [67] with an essential arginine (aArg210 in *E. coli*) located on helix 4 one turn above the middle of the membrane dielectric. The other subunits of F_0, namely bb′ or b_2 in *E. coli*, are largely α-helical proteins, the two helices of b_2 or bb′ probably form a coiled-coil that stretches out from the membrane, over to and tightly binding to one $\alpha\beta$-cleft and farther up to and again firmly binding to subunit δ (see [68] and references therein). The binding of subunits δ at the very top of $(\alpha\beta)_3$ is very strong, with a dissociation constant of less than 1 nM [69], and b binds with a dissociation constant of 150 nM to one $\alpha\beta$-cleft [70]. The complex of three different subunits, named b, δ, and F_6, which make up the peripheral stalk in MF_0F_1, has recently been crystallized and found to form an extended and supposedly rather rigid double strand of parallel and anti-parallel helices [71]. It is agreed that the peripheral stalk is firmly attached to $(\alpha\beta)_3$ on one side and probably also to subunit a on the other. Whether this linkage is elastically stiff, soft, or even floppy is a matter of debate, but see below.

21.3.2 F1, the Rotary Catalyst

21.3.2.1 Nucleotide Binding Sites and Cooperativity

Paul Boyer developed the concept of an alternating function of at least two catalytic sites on the F_1-ATPase, the binding change mechanism [72]. A rotating mechanism involving three catalytic sites became evident by the X-ray structure [12]. The hexagon of $(\alpha\beta)_3$ incorporates a total of six nucleotide binding sites, three of which are catalytically active. If the affinity of the other three is greatly reduced by mutation, these sites are unoccupied but the enzyme remains functional (see [73] and references therein). The three catalytic sites bind Mg-ATP with negative cooperativity. In a mutant F_1 from *E. coli* with engineered tryptophan residues as reporters of the nucleotide occupancy, the respective dissociation constants are ≤ 1 nM for the first, some 100 nM for the second (with the first one occupied), and some 10–100 μM for the third site (see [74]; for TF_1 see [75]). The "negative binding cooperativity" contrasts with "positive catalytic cooperativity" between these sites; the catalytic constant of uni-site and bi-site catalysis (at very low ATP concentration) is much smaller than the one of tri-site catalysis, which is considered as obligatory by A. Senior and J. Weber [76]. Whether the structural coupling behind those cooperativities is mainly attributable to contacts between subunits α-β-α or rather to the position of subunit γ in α-γ-β contacts is not settled.

Movie 2[§] is a rather free animation of a concerted operation of three catalytic sites in the synthesis direction powered by the proton-driven rotation of the central shaft. These sites are supposed to be equivalent in the time average. During forced turnover each of them cycles over three steps: (i) binding of substrates, Mg-ADP and P, (ii) anhydride bond formation to yield bound Mg-ATP, and (iii) release of the product, Mg-ATP.

Biochemical studies have led to the postulate of a reaction sequence where one nucleotide site is always unoccupied ("bi-site mechanism" *o*pen, *l*ow affinity and a *t*ight site (O-, L-, T-site) [72,77]. They were later coined βE, β*D*P and β*T*P because the crystal structure [12] showed one site *e*mpty, one filled with A*D*P, and the third filled with AMPPNP (thought to mimic A*T*P). Thus the crystal structure seemingly supports bi-site functioning. Whether or not there is a real discrepancy between structural and biochemical data is not quite clear. The crystals have been grown in the presence of the bactericide azide, which promotes ADP-inhibition, and, therefore, they are built from the ADP-inhibited and not from the working enzyme. However, mutant enzymes with engineered tryptophans as fluorescent reporters of nucleotide occupancy may have altered affinities for nucleotides. This matter has remained open.

Figure 7 illustrates a tri-site version of the binding change mechanism. It involves three filled sites that change their states of affinity between *l*ow,

[§]Animation of the proton driven F_0F_1 ATP synthase (2005 by iAS, courtesy of IWF.de). The movie can be viewed at www.bioligie.uni-osnabrveck.de/biophysik/junge, with permission of Prof. Wolfgang Junge.

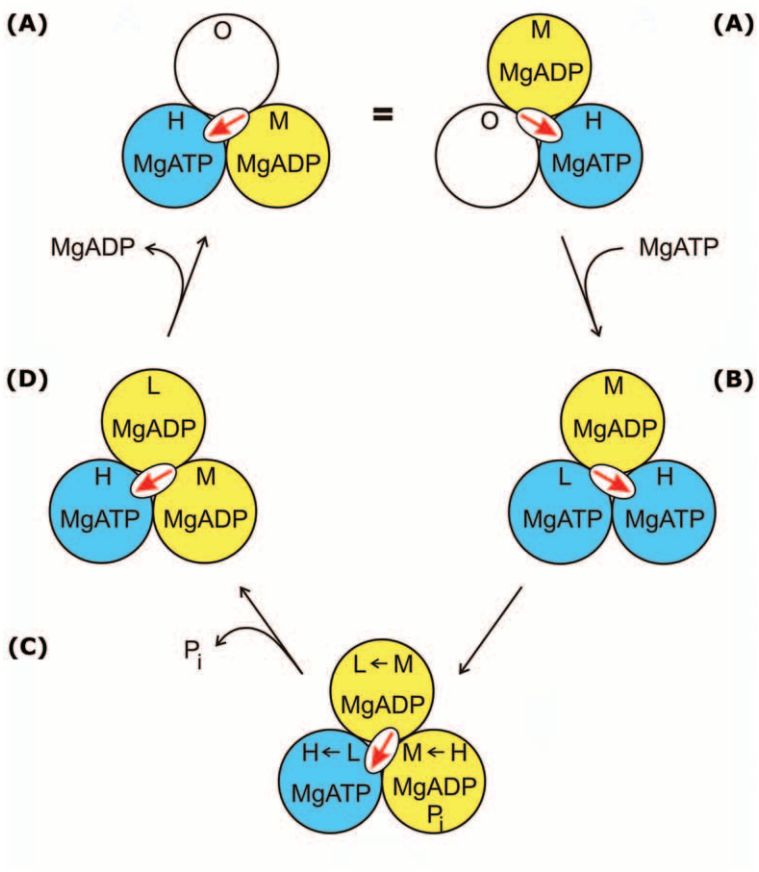

Figure 7. Schematic representation of the rotary binding change mechanism in ATP hydrolysis, after [78] (see text).

*m*edium and *h*igh (L-, M-, H-site) [78]. Hydrolysis of ATP rotates the central shaft (red arrow) over 120°, which is divided into two rotary sub-steps, the first one initiated by the hydrolysis of bound ATP and the second one, claimed in this model, by the release of phosphate (see Section 21.3.2.2 for biophysical evidence on which step generates torque). The very steps that generate torque in F_1 (in the model shown in Figure 7, the cleavage of bound ATP and the release of phosphate) are the ones that drive proton pumping by F_0F_1 (see below).

21.3.2.2 Rotations

A rotary mechanism of ATP hydrolysis by F_1 was plausible as soon as the first asymmetric crystal structure revealed the still picture of a molecular Wankel engine. The first to catch the enzyme "in flight" was Richard Cross' group [14].

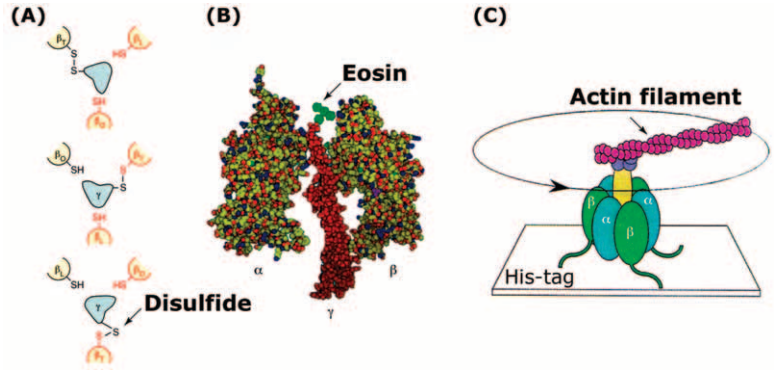

Figure 8. Three techniques to detect inter-subunit rotation in F_1 [66] (see text).

They relied on crosslinking two engineered cysteines in subunits β and γ (Figure 8A). Assembling EF_1 from a disulfite linked βγ-pair (black-black in Figure 8) plus two "hot" copies of subunit β (red), they found that the cleavage and the subsequent reformation of the SS-bridge produced new βγ-pairs (red-black) if the enzyme hydrolyzed ATP, but the same pair if it was inactive. Their conclusion was that the cysteine on subunit γ could be linked to its partner cysteines on all three copies of β. They found a similar result for the reassembled EF_0F_1 under ATP synthesis [79].

The author's group embarked on time resolving the rotation by a spectroscopic probe attached to the penultimate amino acid, a cysteine, of chloroplast CF_1 (Figure 8B). The enzyme was immobilized on an ion-exchange gel and the rotation of the dye eosin recorded by polarized laser photo-bleaching and recovery [15,80]. Three phases of rotation were detected: (i) A very rapid and range-limited librational motion of the long axis of the chromophore in nano-seconds (librational diffusion around the single bond of the dye's attachment, with the range limited by protein contacts), (ii) further rotational relaxation in about 30 μs (again libration around the single bond, with the range widened by protein conformational changes in some ten μs), and (iii) a slow phase (of about 100 ms duration) that was only observed if the enzyme was hydrolyzing ATP. The rotational relaxation time conformed with the enzymatic turnover time under the given conditions [82,83]. The monotonic decay of the polarization anisotropy implied that the rotation was stepping with two or three but not more steps [80].

Whereas the first approach lacked time resolution and both the first and second lacked information on the direction of rotation, the third approach by the groups of Masasuke Yoshida and Kazuhiko Kinosita had it all (Figure 8C). An engineered TF_1 was fixed by His-tags to a Ni-coated solid support, a fluorophore-labeled actin-filament was attached to the C-terminal end of subunit γ, and the position of the filament recorded by video-microscopy. Under conditions of ATP hydrolysis they observed the counter-clockwise rotation, viewing from the membrane side of F_1 [16]. It conformed with the

expected sequence of events based on the asymmetric crystal structure, namely that the convex side of subunit γ progresses from facing βE via βDP to βTP [2]. A filament of typical length 2 μm is over 100× longer than the diameter of the enzyme (≈10 nm), its motion is overdamped by viscous drag such that substeps are not detectable, and the enzyme turnover is slowed down from milliseconds to seconds. To overcome the rate limitation by viscous drag the same laboratories used 40 nm gold beads on subunit γ as reporter and recorded the rotational speed at high speed (8000 video-frames per second) [81]. The large size of the diffraction limited spot of the bead (width ≈300 nm) was not deleterious because its centroid position was more sharply defined owing to the eccentric mounting on the enzyme via BSA.

Figure 9 illustrates the experimental set-up and documents the stepping of the eccentric spots. The stepping length was 120°, as expected, with two substeps of 90° and 30°. The 90° step was at least triggered if not driven by the binding of ATP, the 30° step was independent of ATP. Both steps were rapid, taken together they were completed in less than 250 μs (at saturating ATP). That the "interim dwell", 2 ms, was shorter than the apparent turnover time of 7.7 ms in solution (turnover number 130 s^{-1}) was attributed to the difference between single molecule experiments (detecting the behavior of active enzyme

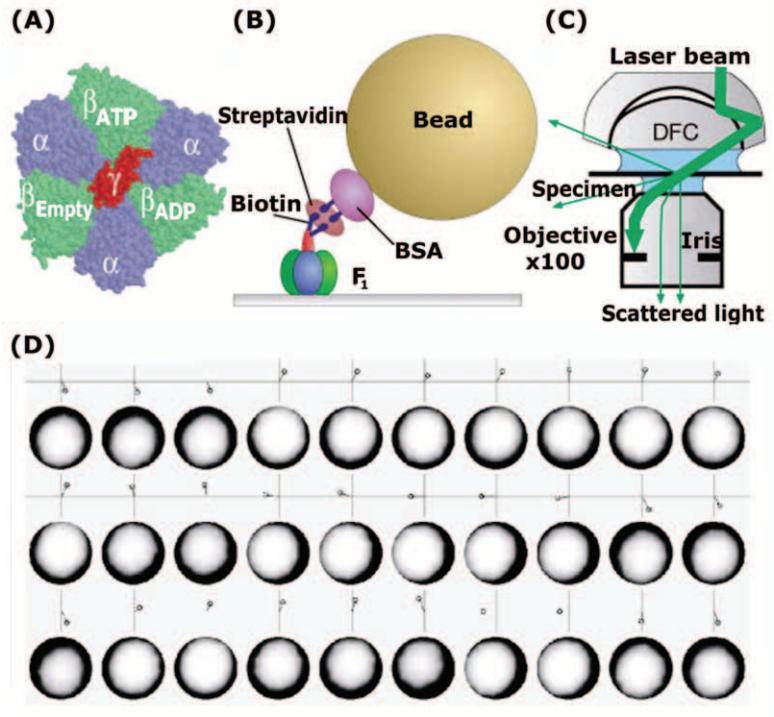

Figure 9. Recording of the rotary dynamics of rotary F_1-ATPase using 30 nm gold beads in dark-field microscopy and a high-speed video-camera [81] (see text).

molecules) and ensemble experiments (detecting the mean behavior of active and inactive ones) [81]. The same laboratories later revised the width of the substeps into 80° and 40° intervals and assigned one of the "interim dwells" to the cleavage of ATP [82] and to product release [83], respectively. The latter study with fluorescent nucleotide analogues supported a tri-site (Figure 7) over a bi-site mechanism.

Spectroscopic rotation assays have been refined as well. Polarized confocal microscopy applied to immobilized single molecules yielded the first evidence for three stepped rotary progression of subunit γ [84]. The first to prove rotation in the membrane bound enzyme, were Peter Dimroth and his colleagues. They used PF_0F_1-proteoliposomes, fixed by the enzyme on a solid support, and recorded the rotating polarization of a dye molecule that was covalently linked to subunit c. It revealed the rotation of the c-ring not only in the direction of ATP hydrolysis but also for Na^+-driven synthesis [85]. Peter Gräber's group used fluorescence resonance energy transfer (FRET) to monitor the distance between two chromophores, one attached to the rotor and the other one to the stator of EF_0F_1. Reconstituted in proteoliposomes, they monitored transients of the resonance energy transfer during the rather long passage time of the liposome, the femto-liter focal spot of a confocal microscope, and observed the stepped rotation in either direction – synthesis and hydrolysis of ATP [86,87]. Confocal single-molecule FRET is hampered, like other single-molecule fluorescence techniques, by a poor signal-to-noise ratio. This is because organic fluorophores bleach after absorption of only 10^5 quanta of light. Quantum dots do not, but their size, some 10 nm, is not appropriate for sampling small distances within a protein.

If any doubt as to the rotary function of F_1 both in hydrolysis and synthesis was left, it became obsolete by the following experiment: Hiroyasu Itoh et al. [88] attached a magnetic bead to subunit γ of immobilized TF_1, rotated an externally applied magnetic field and detected ATP production by chemiluminescence of luciferin-luciferase. Straightforward as it sounds, this experiment was a tough piece of work. The reduction of volume to minimize the dilution of ATP and background photons were major challenges.

21.3.2.3 Torque and Thermodynamic Efficiency

The average angular velocity of a rotating fluorescent actin-filament was used to estimate the average torque produced by F_1 during ATP hydrolysis. In doing so it was assumed that the angular velocity is limited by viscous drag, that the filament can be approximated as a straight cylindrical rod, and that this rod is exposed to the viscosity of the bulk medium. The torque (M) is then given by eqn. (5), wherein ω denotes the angular velocity and Γ the drag coefficient:

$$M = \Gamma\omega \tag{5}$$

Consider a thin, long cylinder (length L, radius r) rotating in an unbound fluid (viscosity η). If the rotation is perpendicular to the long axis of the cylinder

and fixed to one end the drag coefficient is approximately (see [89,90]):

$$\Gamma \cong \frac{4\pi}{3} \cdot \frac{\eta \cdot L^3}{\ln\left(\frac{L}{r}\right) - 0.447} \tag{6}$$

In their pioneering paper, H. Noji et al. [16] arrived at the conclusion that the torque amounts up to 40 pN nm. When sustained over an angle of $120^\circ = 2\pi/3$, the progression per ATP molecule hydrolyzed, this torque implies a molar mechanical work of 50 kJ mol^{-1}, which is less than the calculated free energy of ATP hydrolysis under their conditions (72–87 kJ mol^{-1}, see [91]). Still, it was taken to indicate nearly 100% efficiency of F_1-ATPase [92,93]. H. Noji et al. [16] were aware of a possible underestimation of the torque. An actin filament (e.g., 2 μm long, 5 nm thick) anchored to a rotating shaft sticking out at a height of about 10 nm over a surface does not "feel" the viscosity of the unbounded bulk solution but a greater one, because of flow coupling to the surface, not to mention surface friction and obstacles. The single molecule observation of rotation by filaments, though spectacular, is actually restricted to a very small fraction, 0.1–1%, of typically 100 filaments in the microscope field. ATP-driven rotation is often obstructed, not only by ADP-inhibition of the enzyme but also by surface contacts. Rotary trajectories with a constant slope (used to calculate the torque) are highly selected examples.

Figure 10 illustrates an alternative way to determine the torque. It avoids the above complications. The actin-filament is used as a spring-balance and the torque is gauged by its elastic deformation [94–96]. The bending of filaments at given torque depends very little on whether the counter-torque is due to viscous drag, surface friction or blockade of the filament by an obstacle [96]. This technique was applied to monitor the torque profile generated by ATP hydrolysis in EF_0F_1 with the filament specifically attached to the c-ring of F_0 (Figure 10C) [95]. The first row (Figure 10A) of video frames (40 ms exposure each) shows a rotating filament 3.2 μm long (see Movie 3[¶] for an original record). The filaments curvature is obvious. The second row (Figure 10B) shows the same filament, now stalled. That it is still curved implies torque generation by the enzyme despite stalling, probably by hitting an obstacle. The torque can be calculated from the curvature once the flexural rigidity of the filament is known. It follows from the variance of thermal fluctuations of the filament tip (see [11]). A figure of 10^{-25} Nm^2 was the typical rigidity [95]. Figure 11 shows the resulting profile of the torque as a function of the angle. The mean was 50 ± 6 pN nm. In the same set of experiments the torque calculated from the angular velocity of rotation [eqn. (5)] was much smaller, only 20 pN nm, revealing the inadequacy of torque determination from the rate of rotation.

Torque (M) times the angular displacement per ATP molecule ($\delta\Phi = 2\pi/3$) gives the mechanical work (ΔW) done on the filament. The molar mechanical

[¶] Original video of rotating filament of 3.2 mm length attached to the c-ring of immobilized F_0F_1 as illustrated in Figure 10(C) (95). The movie can be viewed at www.bioligie.uni-osnabrveck.de/biophysik/junge, with permission of Prof. Wolfgang Junge.

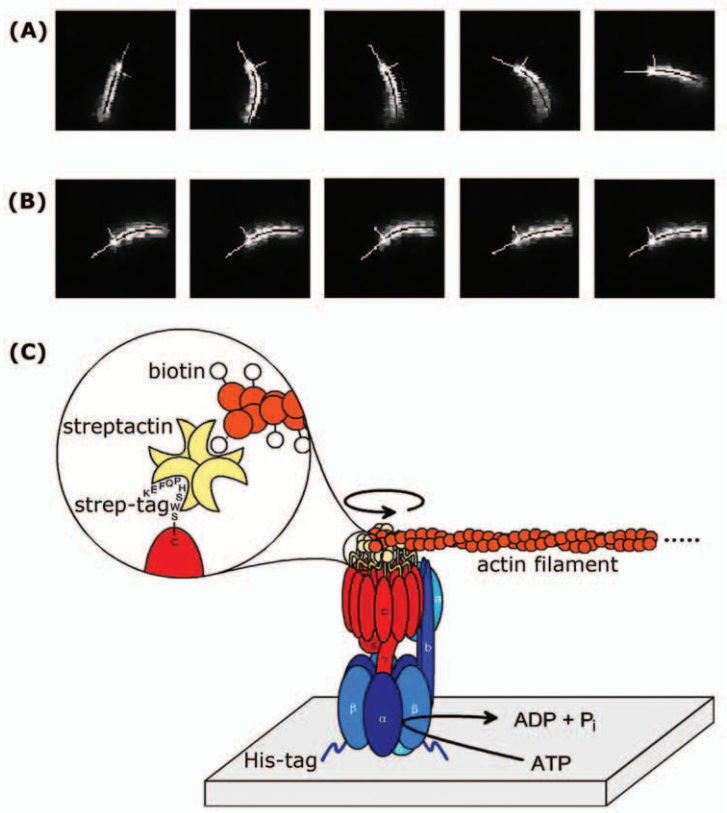

Figure 10. Rotary F_0F_1-ATPase with attached actin filament (length 3.2 μm). Enzyme turnover is several orders of magnitude slower than without filament, which is curved by the enzyme torque. The curvature of the filament has been used as a rotary spring balance to gauge the torque independent of the magnitude of viscous drag and of the interference of surface obstacles [94–96]. (A) Rotating enzyme with attached filament bent by viscous drag. (B) Stalled enzyme by blocked filament contacting an obstacle on the surface, the enzyme torque still bending the filament. (C) Specific attachment of actin filament to the c-ring of detergent solubilized and immobilized EF_0F_1 [108].

work is:

$$\Delta W = M \cdot \frac{2\pi}{3} \cdot N_A \tag{7a}$$

where N_A denotes the Avogadro number.

A mean torque of 50 pN nm implies a molar work of 63 kJ mol^{-1}. This figure matches the calculated free energy of ATP hydrolysis in these experiments:

$$\Delta W = M \cdot \frac{2\pi}{3} \cdot N_{\mathrm{A}} = -\Delta G_{\mathrm{P}} = -\Delta G^{\circ}_{\mathrm{P}} - RT \ln \frac{[\mathrm{ADP}] \cdot [\mathrm{P}] \cdot [\mathrm{H}^+]}{[\mathrm{ATP}]} \tag{7b}$$

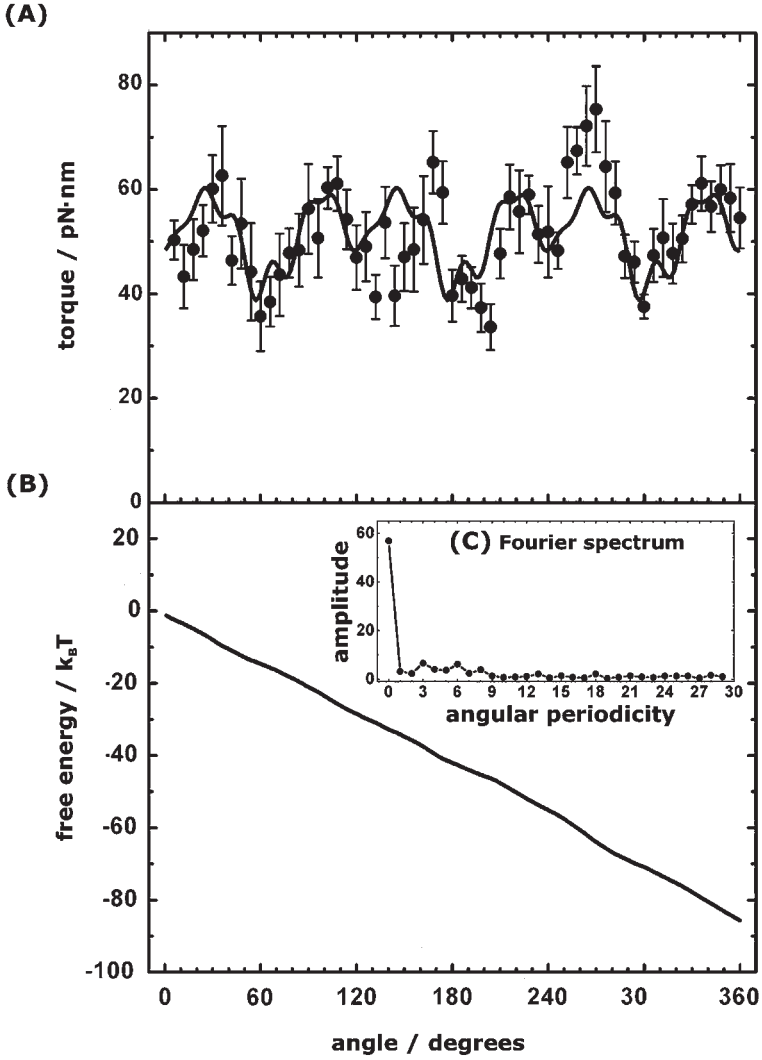

Figure 11. Torque and free-energy profile of EF_0F_1 determined by the curvature of a long actin filament attached to the c-ring of EF_0 [95].

It implies that the enzyme indeed operates at 100% efficiency [94,95]. The 100% efficiency under these conditions has been considered as a particular achievement, which it is not really. A filament 3 μm long reduces the rate of ATP hydrolysis from $>100\,s^{-1}$ in the free enzyme to less than $1\,s^{-1}$. The rotating enzyme thus operates slowly and close to equilibrium, as documented in Figure 10(A), if not truly in thermodynamic equilibrium when stalled by an obstacle (Figure 10B). Because the internal friction is negligible, the thermodynamic efficiency between filament deformation and enzyme chemistry is, trivially, expected to be 100%. A better way to appreciate this efficiency is to

say, "there is no slip in the power transmission between the chemical reaction site and the proton translocating c-ring".

The above considerations [eqn. (7b)] give the thermodynamic view of the chemo-mechanical transducer F_1. It is approximated if the enzyme turns over much more slowly under a heavy load than it would if free. In eqn. (7b) the right-hand term is the entropic contribution to the free energy; it contributes to the torque only if the on/off-rates of educts and products are higher than the enzyme rotates, so that educts and products are in equilibrium. What about the torque produced under kinetic limitation, far away from the equilibrium? K. Kinosita and colleagues have investigated this situation. They recorded the rotation rate as function of the ATP-concentration ranging from nano- to milli-molar, using objects of different sizes to vary the load on the enzyme [97]. The results were discussed in terms of Michaelis–Menten's description, which relates the reaction velocity (v) to the substrate concentration (here [ATP]) by two parameters, the Michaelis-constant (K_m) and the maximum velocity (v_m):

$$v = v_m \cdot \frac{[ATP]}{([ATP] + K_m)} \text{ and at limiting } [ATP] \ll K_m \tag{8a}$$

$$v \cong \frac{v_m}{K_m} \cdot [ATP] = k_{on}^{app} \cdot [ATP] \tag{8b}$$

At saturating ATP concentration they found v_m determined by the magnitude of the torque and the viscous drag as expected [eqns. (5–7)]. However, K_m varied accordingly so that the apparent rate constant of ATP binding, k_{on}^{app}, of $\approx 2 \times 10^7\,\text{M}^{-1}\text{s}^{-1}$ remained almost constant among enzymes with different load and in the wide concentration range 1 nM to 100 μM ATP [97]. The latter was not quite expected in view of the site-site-cooperativity. But, above 1 nM concentration, there was no indication for switching from one mechanism of rotation to another, from uni- via bi- to tri-site catalysis. As an obvious consequence the possible functioning by a tri-site mechanism calls for dissociation constant below 1 nM for the first two binding sites. There is a clear discrepancy between this figure [97] and the dissociation constants determined by engineered tryptophans as engineered reporter group in the binding pockets [75].

At nanomolar ATP-concentration the rotion is stepped. During occasional 120°-jumps the same angular velocity, i.e., the same torque, was observed at 2 nM ATP as in the average under saturating 2 mM ATP [97]. Let us consider an enzyme waiting some ten seconds for the next ATP molecule to bind (the rate being $4 \times 10^{-2}\,\text{s}^{-1}$ at 2 nM ATP). In the very moment when an ATP molecule happens to jump (diffusion controlled) into the receptive binding site the enzyme is certainly not in equilibrium with the nucleotides in the solution. The torque produced during the sudden jump into the next angular position that follows cannot depend on the entropic term on the right-hand side of eqn. (7b). Pulsed torque under ATP-limitation is not expected to be the same as the one detectable in thermodynamic equilibrium. Why it seems to be of equal magnitude, whether by chance or not, has remained an open question.

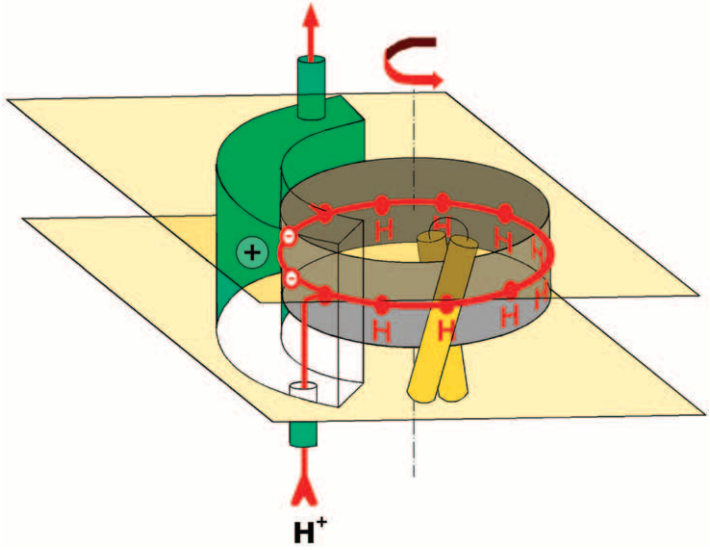

Figure 12. (A) Schematic representation of the rotary electromotor, F_0 [66].

21.3.3 F_0, the Rotary Electromotor

21.3.3.1 Concept of Rotary Proton Transport

Figure 12 illustrates a model for how proton transport may be coupled to torque generation. It incorporates both essential elements, the homo-oligomeric ring of c-subunits, each hairpin shaped and with an acid residue in the middle of the membrane, and the a-subunit with the essential positive arginine. This model has several fathers. Conceived by the author in 1992 and discussed at several conferences since 1993 (see [66]), it was independently conceived by Steve Vik [98] and has been theoretically treated by statistical mechanics by George Oster and colleagues [99,100] and Dmitri Cherepanov in the author's laboratory [30].

The following simple principles of operation are agreed on: (1) The c-ring carries out rotational diffusion relative to the a-subunit. (2) This stochastic librational motion is restricted by two electrostatic constraints, namely that the essential acid residue must be (a) deprotonated when facing the positive arginine residue on subunit a and (b) protonated when facing the lipid core. (3) There are two non-collinear access channels for protons from either aqueous phase leading to acid residues on the c-ring. The electrostatic constraint related to the arginine in subunit a prevents short-circuiting of proton flow and, together with the two non-collinear channels, it conveys chirality to the electromotor. Movie 4[‖] illustrates the back and forth fluctuation of the c-ring

[‖] Animation of the rotary electromotor, F_0 (2001, M. Sauer and W. Junge). The movie can be viewed at www.bioligie.uni-osnabrveck.de/biophysik/junge, with permission of Prof. Wolfgang Junge.

relative to subunit a, which is constrained by electrostatic penalty until a proton coming from the lower phase binds to a negatively charged residue and relieves the constraint. This allows the progression of the ring by one step in the counter-clockwise direction. The same step brings a proton at the other end of the ring in contact with the exit channel, so that it leaves into the upper phase. In this view the rotary drive counts and compares the probability of proton entry from either side – it is an entropic ratchet. This simple model describes equally well torque generation by proton transfer and proton pumping by applied torque.

The model belongs to Brownian ratchets, which have been amply discussed in the context of other motor proteins. As discussed in Richard Feynman's textbook on physics [101], it is a misconception that they are Maxwell demons that perform useful work based on thermal fluctuations. Figure 13 illustrates an archetypal ratchet. A particle diffuses asymmetrically in a saw-tooth potential but it is essentially kept in place while the potential is on. When the potential is off this constraint is relieved, and the diffusion is symmetrical. When the potential is switched on again the particle drifts. The drift is asymmetrical because of the saw-tooth shape of the potential, and it causes directed transport. The energy input for transport is supplied by gearing up the potential but not by Brownian motion. Compared with this classical ratchet with periodical energy input, the above model for the electromotor of F-ATPase is an entropic ratchet, where different probabilities of proton entry from the lower and the

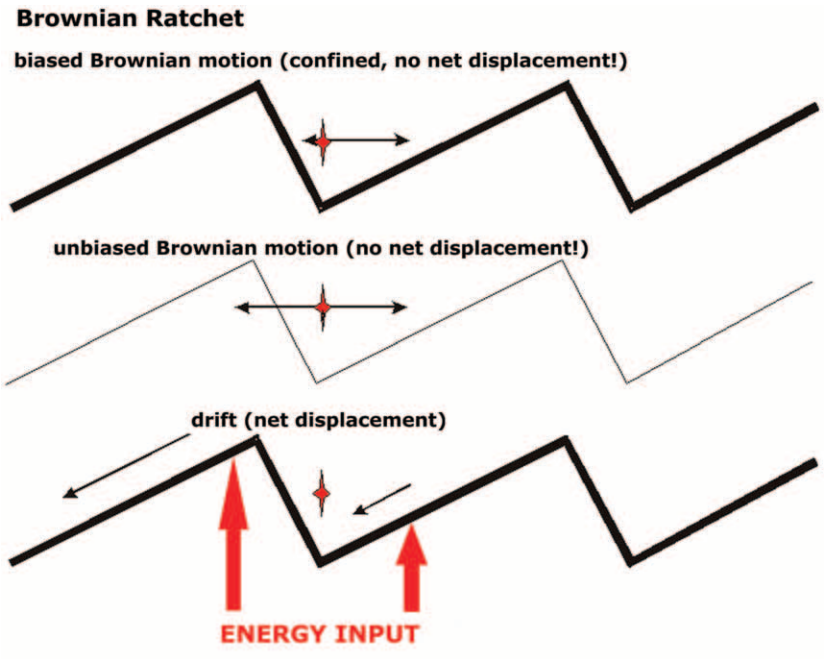

Figure 13. Brownian ratchet mechanism (see text).

upper phase, respectively, determine the direction of rotation and produce work. The model for F_0 is basically conceived to sample the entropic term ($RT\ln[H^+]$) of the free energy of the proton.

How does the transmembrane voltage come into play? One concept has been based on the assumption that the two access channels are monospecific for protons [66]. Obviously, a voltage difference of 120 mV between the two phases will decrease the pH at the central acid residue by one unit when viewed towards the plus side and increase it by the same amount viewing towards the negative side. Then we are back to the entropic ratchet.

Two modifications to the above simple mechanisms of rotary ion transport have been discussed in the literature (see [102] and references therein). (i) Bob Fillingame – based on seemingly conflicting structural data obtained by solution NMR of the c-monomer, on the one hand, and by cysteine-mapping of the c-ring, on the other – proposed a model where the c-ring was not rotating as a stiff entity but with obligatory swiveling of the hairpin-helices when in contact with subunit a [103]. The recent crystal structure of the c-ring of *I. tartaricus* [60], however, deviates from the one inferred from solution NMR of *E. coli* subunit c. Because the arrangement of helices is now compatible with the one from cysteine-mapping, i.e., a swiveling mechanism no longer needs to be invoked. (ii) An asymmetric position in the membrane of the acid residues on the c-ring was claimed, based on several lines of circumstantial evidence, and it led Peter Dimroth to postulate a ''one-channel model'' [104] as opposed to the ''two-channel model'' shown in Figure 12. Again this topology is not supported by the crystal structure [60].

The question of whether or not the c-ring rotates together with subunits γ and ε relative to the stator subunits has been positively answered by cross-linking subunit c with subunit ε without loss of function in EF_0F_1 [65,105] and by video-micrographic rotation assay [106–108].

21.3.3.2 Proton Conductance of F_0

The magnitude of the proton conductance of F_0 has been under debate for mainly two reasons, (i) inadequate resolution of the pH-detector (e.g., glass electrodes) and (ii) uncertainty about the number of active F_0 in the assay chamber. This has led to both under- and overestimation of the conductance by orders of magnitude. Another factor is that a rotary proton carrier like F_0 is expected to show a conductance of femto- rather than pico-Siemens ($10^{-12}\,A\,V^{-1}$) at physiological pH. This has prevented the application of the patch-clamp technique (resolution of pS) to the proton conduction of single copies of F_0.

A solution was found by spectroscopic techniques using the inbuilt ''molecular voltmeters'' of photosynthetic membranes (see pioneering study in [109]). Chromatophore vesicles of a purple bacterium were prepared to such small size (diameter 30 nm) that they contained only about 0.3 copies of F_0 on the average (F_1 removed). This allowed the determination of the unitary conductance in the subset of vesicles containing a single copy of F_0 [30]. These mini-chromatophores contained the full complement for the primary processes of

photosynthesis, i.e., about 10 copies of the bacterial reaction centre and the cytochrome bc_1-complex. A sudden jump of the transmembrane voltage (magnitude about 70 mV) was generated by flashing the chromatophores with a 2 ns laser, and the decay of the voltage was monitored spectrophotometrically by electrochromic absorption changes of intrinsic pigments, serving as a molecular voltmeter with high time resolution [25–27]. The relaxation time of the voltage was about 2.2 ms in vesicles with F_0 and was several orders of magnitude longer after the proton conduction by F_0 was specifically blocked. The calculated unitary proton conductance of BF_0 is 10 fS, which, at a voltage of 100 mV, implies 6240 protons transported per second. The conductance is ohmic, and the proton specificity is extremely high. At pH 8 and against a background of 100 mM of K^+ or Na^+ the rejection factor is 10^7. Despite the very high specificity the pH-dependence is rather low, in the wide pH range 6.5–10 it varies only by a factor of two [30]. This behavior was simulated by statistical mechanics in terms of the rotary transport model of Figure 12. The simulation required only three free parameters, including two different p*K*-values in the access channels (6.1 and 10, respectively). The least that can be said is that the rotary model is compatible with the observed conductance of F_0 [30]. How does the conductance of F_0 compare with the conductance of gramicidin A? It has been determined in the pH-range 0–4 units [110]. Extrapolated to pH 8 the expected proton conductance of gramicidin A is only 1 fS; this is tenfold lower than that of F_0, which is astounding in the light of the required rotation in the latter.

How does the conductance of F_0 compare with the conductance of the coupled enzyme, F_0F_1? The typical rate of ATP synthesis under high proton-motive force (say at 200 mV) is $300\,s^{-1}$ or 100 rps. With a C_{10}-symmetrical c-ring the rate of proton transport is $1000\,s^{-1}$, which is by one order of magnitude less than the expected rate of proton transport by free F_0 ($>10000\,s^{-1}$ at 200 mV). Thus, F_0 operates as a low-impedance motor for the chemical generator, F_1.

21.3.4 F_0F_1, the Rotary Twin-Engine

21.3.4.1 Fine-Tuning Versus Robustness

The ATP synthase, F_0F_1, is a paradigmatic enzyme that has it all, a rotary electro-motor, a mechanical power transmission and a rotary chemical generator. How do they work together? Is one particular reaction step in one component, e.g., the passage of one proton through F_0, fine-tuned to a corresponding step in the other portion, e.g., the breaking of one particular hydrogen bond in F_1? The evidence clearly favors a robust over a finely tuned operation of this enzyme (see [94]).

Both its motor/generators are steppers. Their symmetries, C_3 and $C_{10,11,14}$, respectively, do not match in some organisms, but they do, C_3 versus C_{15}, in at least one. Sequence alignments between related subunits from different species show high similarity for a few key domains, e.g., the nucleotide binding pockets between $\alpha\beta$ and the ion-binding domain on c, but very low similarity between

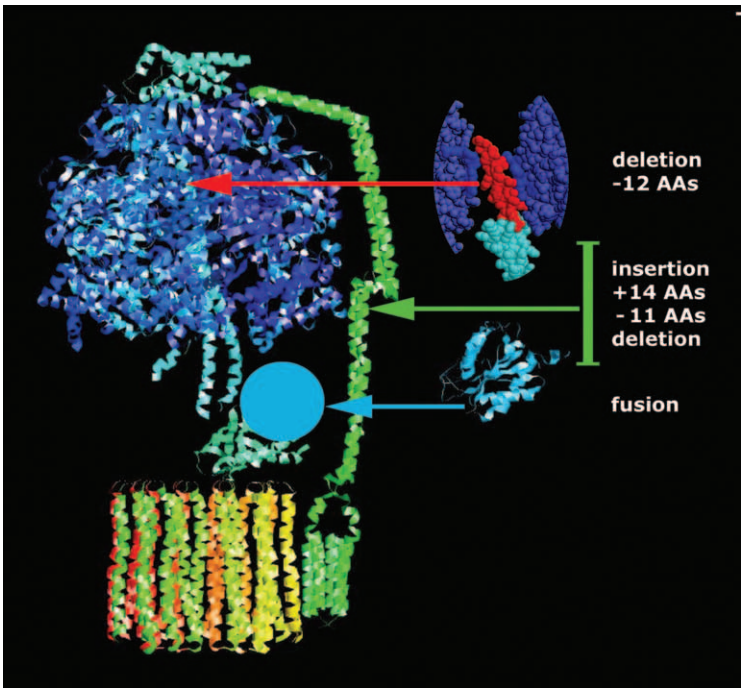

Figure 14. Robustness of the F_0F_1-ATP synthase; gross structural modifications without that EF_0F_1 loses its function. (i) Deletion of twelve C-terminal amino acids (marked in red) that normally anchor subunit γ in the "hydrophobic bearing" (dark blue) of $(\alpha\beta)_3$ [69]. (ii) Insertion of 14 or deletion of eleven residues from subunit b (the total length difference marked in green) [96]. (iii) Genetic fusion of flavodoxin light blue into subunit ε [14].

those portions and subunits involved in the mechanical action (e.g., only 13% sequence identity for δ between spinach chloroplasts and *E. coli* [111]). Figure 14 illustrates three types of severe structural alterations of the *E. coli* enzyme that do not inactivate the enzyme. (i) The deletion of 3–12 residues at the C-terminus of subunit γ neither impairs ATP hydrolysis by solubilized F_1 nor the ability of the fixed enzyme to generate torque and to drive an actin filament around [112]. This stretch on γ – shown in red in Figure 14 – supposedly holds the rotating shaft in its hydrophobic bearing (shown in dark blue). (ii) Insertion of 14 residues or deletion of 11 in subunit b – the length-difference of 25 given as a green bar in Figure 14 – does not impair the ability to perform proton-coupled ATP hydrolysis and synthesis [113,114]. (iii) The fusion of flavodoxin – shown in light blue – to subunit ε left EF_0F_1 functional as well [115]. Another wild construct, the chimeric enzyme, PF_0EF_1, gene-fused from α, β, γ, and ε of *E. coli* and subunits a, b, c, and δ of *P. modestum* is fully functional and displays the Na^+-translocation of its PF_0 portion [116]. The fusion of two, three [117] or five and ten copies of subunit c [63] in the rotor ring of bacterial enzymes is likewise tolerated. From the above, clearly, the two motor/generators of ATP

synthase have not been coupled into a "finely tuned machine" as suggested by some. The question is what makes this enzyme so tolerant against gross structural modifications and change of gear in different organisms?

21.3.4.2 Elastic Power Transmission

The robustness of the function has fostered speculation on an elastic power transmission between and within F_0 and F_1 [118,119]. Kinetic modeling of proton transport and ATP synthesis seemed to support this view [66,93]. Conceivably, the rotor, with subunit γ as a torsion spring, stores elastic energy provided by proton transport though F_0 and the peripheral stalk acts as an elastic counter-bearing. What is the evidence?

Figure 10(C) shows the experimental set-up to address this question. The enzyme is fixed on a solid support and hydrolyses ATP in a stepwise progression by 120°. Stepping implies discrete peaks of the torque (in loose terms power strokes). An actin filament is specifically bound to the c-ring by engineered step-tags [108]. It is exposed to the discrete torque pulses but its motion is overdamped, so that the free end does not immediately follow the jumps of the driving motor. It rotates quasi-continuously, and the stepping of the driving motor is blurred (see [96] for the theory). Because of the slow motion under heavy load (approximating thermodynamic equilibrium, as discussed above) the momentary torque is reflected by the filament's curvature. Curvature analysis revealed the rather flat torque-profile shown in Figure 11(A) [95], a minor period of 3 over 360°-rotation, was evident from Fourier analysis (see insert in Figure 11B). Integration of torque over the angle yielded the work output at the c-ring (Fig 11B), a rather straight line here calibrated in units of k_BT. Over 360° it covers $83kT$, i.e., $28k_BT$ per ATP-molecule ($67\,kJ\,mol^{-1}$). Why does the stepper motor F_1, which by itself has a strongly undulated energy profile (activation energy of 40–50 $kJ\,mol^{-1}$), deliver an almost linear work profile, i.e., almost constant torque, to its partner motor, F_0? This situation has been analyzed by solving the Fokker–Planck equation for a stepper motor that is elastically coupled to a heavy load [95,96], and the result is illustrated in Figure 15.

The solid line in Figure 15(A) describes the free energy profile of free F_1 over 240°. The free energy difference between two minima reflects the useful work from the hydrolysis of ATP. When the enzyme runs downhill to the right it produces torque and delivers heat to the bath. When it runs uphill further to the right, it borrows energy from the heat bath to cross the barrier. If the enzyme is elastically coupled to the load, the elastic element stores the otherwise dissipated energy and flattens the profile, as shown by the broken lines in Figure 15(A). The smaller the torsional rigidity of the power transmission, the straighter the energy profile. [The torsional rigidity (C) relates the torque (M) to the deformation angle (Φ) of a spring (length L) such that: $M = (C/L)\Phi$.]

21.3.4.3 Kinetic Efficiency

The elastic power transmission has important consequences for the performance of rotary engines under load. Figure 15(B) describes the calculated

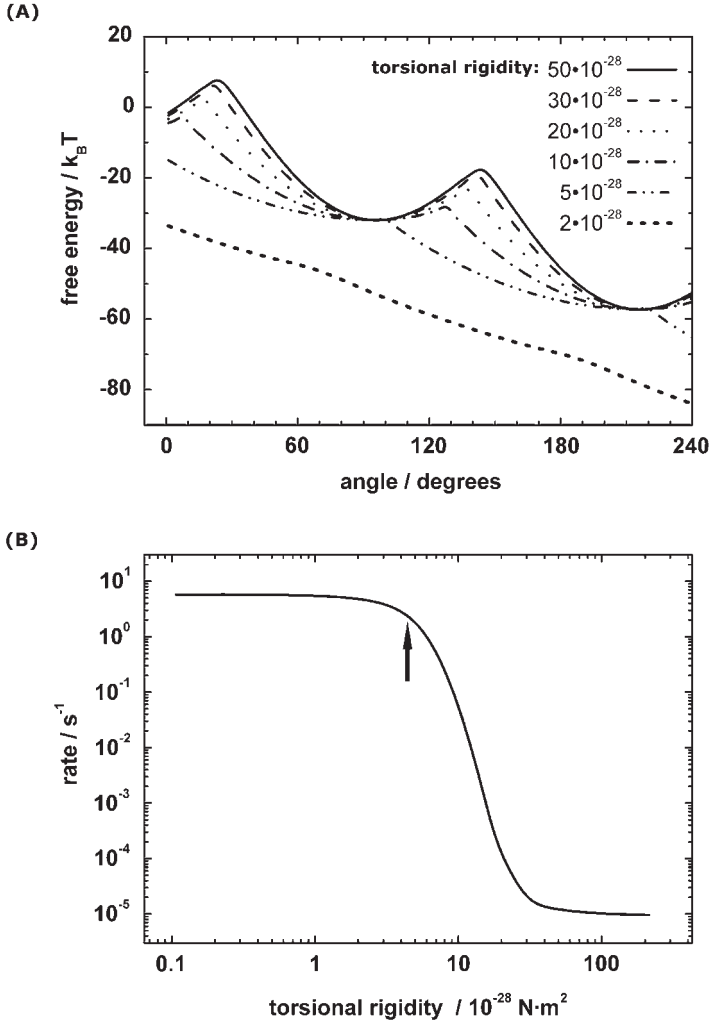

Figure 15. The free energy profile (A) and the turnover rate (B) of a rotary stepper motor as a function of the torsional rigidity of the elastic power transmission to a heavy load [95] (for a detailed description, see text).

rotation rate of the stepper motor F_1 as a function of the torsional rigidity of the elastic power transmission. A high rate requires a soft elastic transmission, whereas a rigid one reduces the rate by orders of magnitude (see [95] for details).

This invokes another efficiency of the enzyme, namely the kinetic efficiency (η_{kin}), as defined by the ratio of the reaction flux (J) over the maximum possible flux (J_{max}):

$$\eta_{kin} = \frac{J}{J_{max}} \tag{9a}$$

as opposed to the thermodynamic efficiency (η_{therm}):

$$\eta_{\text{therm}} = \frac{\Delta W}{-\Delta G} \tag{9b}$$

wherein δW denotes the work done and ΔG the free energy difference of the driving motor.

The thermodynamic efficiency is maximum if the enzyme is stalled, $\eta_{\text{therm}} = 1$, by definition of ΔG. For any realistic turnover of the enzyme the thermodynamic efficiency drops. The kinetic efficiency, on the other hand, can be influenced by engineering. An elastic power transmission straightens the free energy profile to achieve constant torque and high turnover rate. Thus, the elastic coupling is essential for the performance of ATP synthase under physiological conditions. Take, for example, *E. coli*, where the enzyme uses p.m.f. to produce ATP, and, vice versa, uses ATP to restore p.m.f. should it fall low. At the compensation point each of the two motors runs against the heavy load presented by the other one. Whether ATP production or consumption wins is determined by the consumers of ATP and p.m.f. in the cell. This is where an elastic power transmission provides a high turnover rate (Figure 15B). It appears almost as a side effect of the elastic transmission that it guarantees the robustness of function with different gears, using 4.7 protons per ATP in one organism and 3.3 in another. Which physiological conditions call for different gears is not yet clear. Elasticity also accounts for the functioning in structurally modified constructs. ATP synthase is surely not the finely tuned twin-motor as admired by some, it is rather its simplicity and versatility that is beautiful.

The molecular basis of the elasticity power transmission between F_0 and F_1 is the subject of present research. The torsional and flexural compliance of α-helices, the bending or the sequential breaking of hydrogen bonds, and the proportion of elastic energy storage in the central shaft versus the peripheral stalk are interesting questions to follow.

21.4 Outlook

ATP synthase is a paradigmatic enzyme that has it all, an electrical rotary motor, a mechanical power transmission and a rotary chemical generator. ATP synthase is surely not the finely tuned twin-motor as often imagined. Its construction is rather distinguished by simplicity, robustness and versatility – that is its beauty. ATP synthase is among the smallest, surely the most versatile and perhaps the best understood, of nature's nano-engines. With the clear separation of its electrochemical, mechanical and chemical functions, their association with distinct subunits, and with the conservation of these properties over the kingdoms of life the F_0F_1-ATPase has been an ideal target for an integrated attack by molecular genetics (best EF_0F_1), structural biology (best MF_1 and PF_0), rotation assay (best TF_1), and kinetic techniques (best CF_0F_1 and BF_0F_1). It has also been a unique feature that its dynamic behavior over

the major reaction coordinate can almost be followed ''by eye''. Thus ATP synthase presents itself as the appropriate subject for elucidating principles of the electro-mechano-chemical couplings in enzymes. Although it is ''done'' for undergraduate textbooks, it is not for deeper understanding, which is why it will remain a subject of active research over the next decade, in the same way that the bacterial reaction centre, bacteriorhodopsin and even myoglobin have, long after the first principles of their operation were evident.

References

1. D.I. Arnon, M.B. Allen, F.R. Whatley, Photosynthesis by isolated chloroplasts. *Nature* **174** (1954) 394–396.
2. E.C. Slater, Mechanism of phosphorylation in the respiratory chain. *Nature* **172** (1953) 975–978.
3. P. Mitchell, Coupling of photophosphorylation to electron and hydrogen transfer by a chemiosmotic type of mechanism. *Nature* **191** (1961) 144–148.
4. P. Mitchell, Chemiosmotic coupling in oxidative and photosynthetic phosphorylation. *Physiol. Rev*. **41** (1966) 445–502.
5. A.T. Jagendorf, E. Uribe, ATP formation caused by acid-base transition of spinach chloroplast. *Proc. Natl. Acad. Sci. U.S.A*. **55** (1966) 170–177.
6. W. Junge, B. Rumberg, H. Schroeder, Necessity of an electric potential difference and its use for photophosphorylation in short flash groups. *Eur. J. Biochem*. **14** (1970) 575–581.
7. E. Racker, W. Stoeckenius, Reconstitution of purple membrane vesicles catalyzing light-driven proton uptake and adenosine triphosphate formation. *J. Biol. Chem*. **25** (1974) 662–663.
8. H.S. Penefsky, M.E. Pullman, A. Datta, E. Racker, Partial resolution of the enzymes catalyzing oxidative phosphorylation. II. Participation of a soluble adenosine triphosphatase in oxidative phosphorylation. *J. Biol. Chem*. **235** (1960) 3330–3336.
9. P.D. Boyer, The binding-change mechanism of ATP synthesis, in: *Membrane Bioenergetics* (1979) (C.P. Lee, G. Schatz, L. Ernster, eds.), Addison-Wesley, Reading, Mass, pp. 476–479.
10. P.D. Boyer, W.E. Kohlbrenner, The present status of the binding-change mechanism and its relation to ATP formation by chloroplasts, in: *Energy coupling in Photosynthesis* (1981) (B.R. Selman, S. Selman-Reimer, eds.), Elsevier, Amsterdam, pp. 231–241.
11. P.D. Boyer, The ATP synthase – a splendid molecular machine. *Annu. Rev. Biochem*. **66** (1997) 717–749.
12. J.P. Abrahams, A.G.W. Leslie, R. Lutter, J.E. Walker, The structure of F_1-ATPase from bovine heart mitochondria determined at 2.8 Å resolution. *Nature* **370** (1994) 621–628.
13. D. Stock, C. Gibbons, I. Arechaga, A.G. Leslie, J.E. Walker, The rotary mechanism of ATP synthase. *Curr. Opin. Chem. Biol*. **10** (2000) 672–679.
14. T.M. Duncan, V.V. Bulygin, Y. Zhou, M.L. Hutcheon, R.L. Cross, Rotation of subunits during catalysis by *Escherichia coli* F_1- ATPase. *Proc. Natl. Acad. Sci. U.S.A*. **92** (1995) 10964–10968.

15. D. Sabbert, S. Engelbrecht, W. Junge, Intersubunit rotation in active F-ATPase. *Nature* **381** (1996) 623–625.
16. H. Noji, R. Yasuda, M. Yoshida, K. Kinosita, Direct observation of the rotation of F-ATPase. *Nature* **386** (1997) 299–302.
17. L.G. Sillén, A.E. Martell, *Stability Constants of Metal-Ion Complexes* (1964), The Chemical Society, London.
18. R.J.P. Williams, Possible functions of chains of catalysts. *J. Theor. Biol.* **1** (1961) 1–17.
19. R.J.P. Williams, Possible functions of chains of catalysts II. *J. Theor. Biol.* **3** (1962) 209–229.
20. J.F. Nagle, Propaedeutics of ion transport across biomembranes, in: *Ion Transport through Membranes* (1987) (K. Yagi, B. Pullmann, eds.), Academic Press, Tokyo, pp. 181–191.
21. J. Rosing, E.C. Slater, The value of ΔG for the hydrolysis of ATP. *Biochim. Biophys. Acta* **267** (1972) 275–290.
22. S.C. Hinnah, R. Wagner, Thylakoid membranes contain a high-conductance channel. *Eur. J. Biochem.* **253** (1998) 606–613.
23. L.A. Staehelin, *Encyclopedia of Plant Physiology* (1986), Springer-Verlag, Berlin.
24. G. Schönknecht, G. Althoff, W. Junge, The electric unit size of thylakoid membranes. *FEBS Lett.* **277** (1990) 65–68.
25. W. Junge, H.T. Witt, On the ion transport system of photosynthesis – Investigation on a molecular level-. *Z. Naturforsch., Teil B* **23** (1968) 244–254.
26. C. Wolff, H.T. Witt, Metastable states of carotenoids in primary events of photosynthesis. Registration by repetitive ultra-short-flash photometry. *Z. Naturforsch.* **24** (1969) 1031–1037.
27. J.B. Jackson, A.R. Crofts, High energy state in chromatophores of *Rhodopseudomonas speroides*. *FEBS Lett.* **4** (1969) 185–189.
28. H.T. Witt, Coupling of quanta, electrons, fields, ions, and phosphorylation in the functional membrane of photosynthesis. Results by pulse spectroscopic methods. *Q. Rev. Biophys.* **4** (1971) 365–477.
29. W. Junge, J.B. Jackson, The development of electrochemical potential gradients across photosynthetic membranes, in: *Photosynthesis: Energy Conversion by Plants and Bacteria* (1982) (R.A. Govindjee, ed.), Academic Press Inc., New York, pp. 589–646.
30. B.A. Feniouk, M.A. Kozlova, D.A. Knorre, D. Cherepanov, A. Mulkidjanian, W. Junge, The proton driven rotor of ATP synthase: Ohmic conductance, (10fS) and absence of voltage gating. *Biophys. J.* **86** (2004) 4094–4109.
31. P. Mitchell, Proton motive redox mechanism of the cytochrome b-c_1 complex in the respiratory chain: Proton motive ubiquinone cycle. *FEBS Lett.* **56** (1975) 1–6.
32. D.B. Kell, On the functional proton current pathway of electron transport phosphorylation. An electrodic view. *Biochim. Biophys. Acta* **549** (1979) 55–99.
33. S.J. Ferguson, Fully delocalised chemiosmotic or localised proton flow pathways in energy coupling? A scrutiny of experimental evidence. *Biochim. Biophys. Acta* **811** (1985) 47–95.
34. W.A. Cramer, D.B. Knaff, *Energy Transduction in Biological Membranes: A Textbook of Bioenergetics* (1990), Springer-Verlag, New York.
35. R.A. Dilley, Energy coupling in chloroplasts – a calcium-gated switch controls proton fluxes between localized and delocalized proton gradients. *Curr. Top. Bioenerg.* **16** (1991) 265–318.

36. T.A. Krulwich, M. Ito, R. Gilmour, D.B. Hicks, A.A. Guffanti, Energetics of alkaliphilic Bacillus species: physiology and molecules. *Adv. Microb. Physiol.* **40** (1998) 401–438.
37. D.A. Cherepanov, W. Junge, A.Y. Mulkidjanian, Proton transfer dynamics at the membrane/water interface: Dependence on fixed and mobile pH buffers, on the size and form of membrane particles, and on the interfacial potential barrier. *Biophys. J.* **86** (2004) 665–680.
38. D.A. Cherepanov, B.A. Feniouk, W. Junge, A.Y. Mulkidjanian, Low dielectric permittivity of water at the membrane interface: effect on the energy coupling mechanism in biological membranes. *Biophys. J.* **85** (2003) 1307–1316.
39. H.S. van Walraven, H. Strotmann, O. Schwarz, B. Rumberg, The H^+/ATP coupling ratio of the ATP synthase from thiol-modulated chloroplasts and two cyanobacterial strains is four. *FEBS Lett.* **379** (1996) 309–313.
40. P. Turina, D. Samoray, P. Graber, H^+/ATP ratio of proton transport-coupled ATP synthesis and hydrolysis catalysed by CF0F1-liposomes. *EMBO J.* **22** (2003) 418–426.
41. H. Seelert, A. Poetsch, N.A. Dencher, A. Engel, H. Stahlberg, D.J. Mueller, Proton-powered turbine of a plant motor. *Nature* **405** (2000) 418–419.
42. G. Groth, E. Pohl, The structure of the chloroplast F1-ATPase at 3.2 A resolution. *J. Biol. Chem.* **276** (2001) 1345–1352.
43. T. Hisabori, H. Konno, H. Ichimura, H. Strotmann, D. Bald, Molecular devices of chloroplast F(1)-ATP synthase for the regulation. *Biochim. Biophys. Acta* **1555** (2002) 140–146.
44. P. Gräber, The H^+-ATPase from chloroplasts: energetics of the catalytic cycle. *Biochim. Biophys. Acta* **1187** (1994) 171–176.
45. B.A. Feniouk, T. Suzuki, M. Yoshida, The role of subunit epsilon in the catalysis and regulation of F(O)F(1)-ATP synthase. *Biochim. Biophys. Acta* **1757** (2006) 326–338.
46. G. Groth, W. Junge, Proton slip of chloroplast ATPase: Its nucleotide dependence, energetic threshold and relation to an alternating site mechanism of catalysis. *Biochemistry* **32** (1993) 8103–8111.
47. B.A. Feniouk, A.Y. Mulkidjanian, W. Junge, Induction and properties of proton slip in the ATP synthase from Rhodobacter capsulatus. *Biochim. Biophys. Acta-Bioenerg.* **1658** (2004) 109.
48. D. Sabbert, S. Engelbrecht, W. Junge, Functional and idling rotatory motion within F-ATPase. *Proc. Natl. Acad. Sci. U.S.A.* **94** (1997) 4401–4405.
49. M. Bianchet, X. Ysern, J. Hullihen, P.L. Pedersen, L.M. Amzel, Mitochondrial ATP synthase – quaternary structure of the F_1 moiety at 3.6 Å determined by X-ray diffraction analysis. *J. Biol. Chem.* **266** (1991) 21197–21201.
50. G. Groth, Structure of spinach chloroplast F1-ATPase complexed with the phytopathogenic inhibitor tentoxin. *Proc. Natl. Acad. Sci. U.S.A.* **99** (2002) 3464–3468.
51. R.I. Menz, J.E. Walker, A.G. Leslie, Structure of bovine mitochondrial F(1)-ATPase with nucleotide bound to all three catalytic sites: implications for the mechanism of rotary catalysis. *Cell* **106** (2001) 331–341.
52. R. Kagawa, M.G. Montgomery, K. Braig, A.G.W. Leslie, J.E. Walker, The structure of bovine F-1-ATPase inhibited by ADP and beryllium fluoride. *EMBO J.* **23** (2004) 2734–2744.
53. K. Braig, R.I. Menz, M.G. Montgomery, A.G. Leslie, J.E. Walker, Structure of bovine mitochondrial F(1)-ATPase inhibited by Mg^{2+} ADP and aluminium fluoride. *Structure* **8** (2000) 567–573.

54. G.L. Orriss, A.G.W. Leslie, K. Braig, J.E. Walker, Bovine F_1-ATPase covalently inhibited with 4-chloro-7-nitrobenzofurazan – the structure provides further support for a rotary catalytic mechanism. *Structure* **6** (1998) 831–837.
55. J.P. Abrahams, S.K. Buchanan, M.J. van Raaij, I.M. Fearnley, A.G. Leslie, J.E. Walker, The structure of bovine F1-ATPase complexed with the peptide antibiotic efrapeptin. *Proc. Natl. Acad. Sci. U.S.A.* **93** (1996) 9420–9424.
56. Y. Shirakihara, A.G.W. Leslie, J.P. Abrahams, J.E. Walker, T. Ueda, Y. Sekimoto, M. Kambara, K. Saika, Y. Kagawa, M. Yoshida, The crystal structure of the nucleotide-free alpha-3-beta-3 subcomplex of F_1-ATPase from the thermophilic *Bacillus* PS3 is a symmetric trimer. *Structure* **5** (1997) 825–836.
57. J. Hoppe, M. Brunner, B.B. Jorgensen, Structure of the membrane-embedded F_0 part of F_1F_0 ATP synthase from *Escherichia coli* as inferred from labeling with 3-(trifluoromethyl)-3-(m-[125I]iodophenyl)diazirine. *Biochemistry* **23** (1984) 5610–5616.
58. P.C. Jones, W.P. Jiang, R.H. Fillingame, Arrangement of the multicopy H^+-translocating subunit c in the membrane sector of the *Escherichia coli* F_1F_0 ATP synthase. *J. Biol. Chem.* **273** (1998) 17178–17185.
59. M.E. Girvin, V.K. Rastogi, F. Abildgaard, J.L. Markley, R.H. Fillingame, Solution structure of the transmembrane H^+-transporting subunit c of the F_1F_0 ATP synthase. *Biochemistry* **37** (1998) 8817–8824.
60. T. Meier, P. Polzer, K. Diederichs, W. Welte, P. Dimroth, Structure of the rotor ring of F-Type Na^+-ATPase from Ilyobacter tartaricus. *Science* **308** (2005) 659–662.
61. D. Stock, A.G. Leslie, J.E. Walker, Molecular architecture of the rotary motor in ATP synthase. *Science* **286** (1999) 1700–1705.
62. W. Jiang, J. Hermolin, R.H. Fillingame, The preferred stoichiometry of c subunits in the rotary motor sector of Escherichia coli ATP synthase is 10. *Proc. Natl. Acad. Sci. U.S.A.* **98** (2001) 4966–4971.
63. N. Mitome, T. Suzuki, S. Hayashi, M. Yoshida, Thermophilic ATP synthase has a decamer c-ring: indication of noninteger 10:3 H+/ATP ratio and permissive elastic coupling. *Proc. Natl. Acad. Sci. U.S.A.* **101** (2004) 12159–12164.
64. C.L. Tang, R.A. Capaldi, Characterization of the interface between gamma and epsilon subunits of *Escherichia coli* F_1-ATPase. *J. Biol. Chem.* **271** (1996) 3018–3024.
65. B. Schulenberg, R. Aggeler, J. Murray, R.A. Capaldi, The gammaepsilon-c subunit interface in the ATP synthase of Escherichia coli. Cross-linking of the epsilon subunit to the c subunit ring does not impair enzyme function, that of gamma to c subunits leads to uncoupling. *J. Biol. Chem.* **274** (1999) 34233–34237.
66. W. Junge, H. Lill, S. Engelbrecht, ATP synthase: an electrochemical transducer with rotatory mechanics. *Trends Biochem. Sci.* **22** (1997) 420–423.
67. D. Zhang, S.B. Vik, Helix packing in subunit a of the Escherichia coli ATP synthase as determined by chemical labeling and proteolysis of the cysteine-substituted protein. *Biochemistry* **42** (2003) 331–337.
68. S.D. Dunn, D.T. McLachlin, M. Revington, The second stalk of Escherichia coli ATP synthase. *Biochim. Biophys. Acta* **1458** (2000) 356–363.
69. K. Häsler, O. Pänke, W. Junge, On the stator of rotary ATP synthase: the binding strength of subunit delta to, $(\alpha\beta)_3$ as determined by fluorescence correlation spectroscopy. *Biochemistry* **38** (1999) 13759–13765.
70. J. Weber, S. Wilke-Mounts, S. Nadanaciva, A.E. Senior, Quantitative determination of direct binding of b subunit to F1 in Escherichia coli F_1F_0-ATP synthase. *J. Biol Chem.* **279** (2004) 11253–11258.

71. V.K. Dickson, J.A. Silvester, I.M. Fearnley, A.G. Leslie, J.E. Walker, On the structure of the stator of the mitochondrial ATP synthase. *EMBO J*. **25** (2006) 2911–2918.
72. P.D. Boyer, The binding change mechanism for ATP synthase – Some probabilities and possibilities. *Biochim. Biophys. Acta* **1140** (1993) 215–250.
73. J. Weber, A.E. Senior, ATP synthase: what we know about ATP hydrolysis and what we do not know about ATP synthesis. *Biochim. Biophys. Acta* **1458** (2000) 300–309.
74. J. Weber, A.E. Senior, Catalytic mechanism of F_1-ATPase. *Biochim. Biophys. Acta* **1319** (1997) 19–58.
75. H. Ren, S. Bandyopadhyay, W.S. Allison, The $\alpha_3\beta_3$(Met222Ser/Tyr345Trp) gamma subcomplex of the TF1-ATPase does not hydolyze ATP at a significant rate until the substrate binds to the catalytic site of the lowest affinity. *Biochemistry* **45** (2006) 6222–6230.
76. A.E. Senior, J. Weber, Happy motoring with ATP synthase. *Nat. Struct. Mol. Biol.* **11** (2004) 110–112.
77. R.L. Cross, The mechanism and regulation of ATP synthesis by F_1-ATPases. *Annu. Rev. Biochem*. **50** (1981) 681–714.
78. J. Weber, A.E. Senior, ATP synthesis driven by proton transport in F1F0-ATP synthase. *FEBS Lett*. **545** (2003) 61–70.
79. Y. Zhou, T.M. Duncan, R.L. Cross, Subunit rotation in *Escherichia coli* F_0F_1-ATP synthase during oxidative phosphorylation. *Proc. Natl. Acad. Sci. U.S.A*. **94** (1997) 10583–10587.
80. D. Sabbert, W. Junge, Stepped versus continuous rotatory motors at the molecular scale. *Proc. Natl. Acad. Sci. U.S.A*. **94** (1997) 2312–2317.
81. R. Yasuda, H. Noji, M. Yoshida, K. Kinosita, Jr., H. Itoh, Resolution of distinct rotational substeps by submillisecond kinetic analysis of F1-ATPase. *Nature* **410** (2001) 898–904.
82. K. Shimabukuro, R. Yasuda, E. Muneyuki, K.Y. Hara, K. Kinosita, Jr., M. Yoshida, Catalysis and rotation of F1 motor: cleavage of ATP at the catalytic site occurs in 1 ms before 40 degree substep rotation. *Proc. Natl. Acad. Sci. U.S.A*. **100** (2003) 14731–14736.
83. T. Nishizaka, K. Oiwa, H. Noji, S. Kimura, E. Muneyuki, M. Yoshida, K. Kinosita, Jr., Chemomechanical coupling in F1-ATPase revealed by simultaneous observation of nucleotide kinetics and rotation. *Nat. Struct. Mol. Biol* **11** (2004) 142–148.
84. K. Häsler, S. Engelbrecht, W. Junge, Three-stepped rotation of subunits γ and ε in single molecules of F-ATPase as revealed by polarized, confocal fluorometry. *FEBS Lett*. **426** (1998) 301–304.
85. G. Kaim, M. Prummer, B. Sick, G. Zumofen, A. Renn, U.P. Wild, P. Dimroth, Coupled rotation within single F0F1 enzyme complexes during ATP synthesis or hydrolysis. *FEBS Lett*. **525** (2002) 156–163.
86. M. Diez, B. Zimmermann, M. Borsch, M. Konig, E. Schweinberger, S. Steigmiller, R. Reuter, S. Felekyan, V. Kudryavtsev, C. A. Seidel, P. Graber, Proton-powered subunit rotation in single membrane-bound F_0F_1-ATP synthase. *Nat. Struct. Mol. Biol*. **11** (2004) 135–141.
87. B. Zimmermann, M. Diez, N. Zarrabi, P. Graber, M. Borsch, Movements of the epsilon-subunit during catalysis and activation in single membrane-bound H^+-ATP synthase. *EMBO J*. **24** (2005) 2053–2063.
88. H. Itoh, A. Takahashi, K. Adachi, H. Noji, R. Yasuda, M. Yoshida, K. Kinosita, Mechanically driven ATP synthesis by F_1-ATPase. *Nature* **427** (2004) 465–468.

89. A.J. Hunt, F. Gittes, J. Howard, The force exerted by a single kinesin molecule against a viscous load. *Biophys. J.* **67** (1994) 766–781.
90. M.M. Tirado, J. Garcia de la Torre, Rotational dynamics of rigid, symmetrical top macromolecules. Application to circular cylinders. *J. Chem. Phys.* **73** (1980) 1986–1993.
91. R. Yasuda, H. Noji, K. Kinosita, M. Yoshida, F_1-ATPase is a highly efficient molecular motor that rotates with discrete 120° steps. *Cell* **93** (1998) 1117–1124.
92. K. Kinosita, Jr., R. Yasuda, H. Noji, K. Adachi, A rotary molecular motor that can work at near 100% efficiency. *Philos. Trans. R. Soc. London B Biol. Sci.* **355** (2000) 473–489.
93. H.Y. Wang, G. Oster, Energy transduction in the F_1 motor of ATP synthase. *Nature* **396** (1998) 279–282.
94. W. Junge, O. Pänke, D. Cherepanov, K. Gumbiowski, M. Müller, S. Engelbrecht, Inter-subunit rotation and elastic power transmission in F_0F_1-ATPase. *FEBS Lett.* **504** (2001) 152–160.
95. O. Pänke, D.A. Cherepanov, K. Gumbiowski, S. Engelbrecht, W. Junge, Viscoelastic dynamics of actin filaments coupled to rotary F-ATPase: torque profile of the enzyme. *Biophys. J.* **81** (2001) 1220–1233.
96. D.A. Cherepanov, W. Junge, Viscoelastic dynamics of actin filaments coupled to rotary F-ATPase: Curvature as an indicator of the torque. *Biophys. J.* **81** (2001) 1234–1244.
97. N. Sakaki, R. Shimo-Kon, K. Adachi, H. Itoh, S. Furuike, E. Muneyuki, M. Yoshida, K. Kinosita Jr, One rotary mechanism for F_1-ATPase over ATP concentrations from millimolar down to nanomolar. *Biophys. J.* **88** (2005) 2047–2056.
98. S.B. Vik, B.J. Antonio, A mechanism of proton translocation by F_1F_0 ATP synthases suggested by double mutants of the a subunit. *J. Biol. Chem.* **269** (1994) 30364–30369.
99. P. Dimroth, H. Wang, M. Grabe, G. Oster, Energy transduction in the sodium F-ATPase of *Propionigenium modestum*. *Proc. Natl. Acad. Sci. U.S.A.* **96** (1999) 4924–4928.
100. T. Elston, H. Wang, G. Oster, Energy transduction in ATP synthase. *Nature* **391** (1998) 510–514.
101. R.P. Feynman, R.B. Leighton, M. Sands, *The Feynman Lectures on Physics* (1963) Addison-Wesley Publishing, Palo Alto, London, New York.
102. W. Junge, N. Nelson, Nature's rotary electromotors. *Science* **308** (2005) 642–644.
103. R.H. Fillingame, W. Jiang, O.Y. Dmitriev, Coupling H^+ transport to rotary catalysis in F-type ATP synthases: structure and organization of the transmembrane rotary motor. *J. Exp. Biol.* **203**(Pt 1) (2000) 9–17.
104. P. Dimroth, U. Matthey, G. Kaim, Critical evaluation of the one- versus the two-channel model for the operation of the ATP synthase's F_0 motor. *Biochim. Biophys. Acta-Bioenerg.* **1459** (2000) 506–513.
105. S.P. Tsunoda, R. Aggeler, M. Yoshida, R.A. Capaldi, Rotation of the c subunit oligomer in fully functional F_1F_0 ATP synthase. *Proc. Natl. Acad. Sci. U.S.A.* **98** (2001) 898–902.
106. Y. Sambongi, Y. Iko, M. Tanabe, H. Omote, A. Iwamoto-Kihara, I. Ueda, T. Yanagida, Y. Wada, M. Futai, Mechanical rotation of the c subunit oligomer in ATP synthase, (F_1F_0): direct observation. *Science* **286** (1999) 1722–1724.

107. S.P. Tsunoda, R. Aggeler, H. Noji, K. Kinosita, M. Yoshida, R.A. Capaldi, Observations of rotatison within the F_0F_1-ATP synthase: deciding between rotation of the F_0c subunit ring and artifact. *FEBS Lett*. **470** (2000) 244–248.
108. O. Pänke, K. Gumbiowski, W. Junge, S. Engelbrecht, F-ATPase: specific observation of the rotating c subunit oligomer of EF_0EF_1. *FEBS Lett*. **472** (2000) 34–38.
109. G. Schönknecht, W. Junge, H. Lill, S. Engelbrecht, Complete tracking of proton flow in thylakoids – the unit conductance of CF_0 is greater than 10 fS. *FEBS Lett*. **203** (1986) 289–294.
110. S. Cukierman, Proton mobilities in water and in different stereoisomers of covalently linked gramicidin A channels. *Biophys. J*. **78** (2000) 1825–1834.
111. S. Engelbrecht, W. Junge, Subunit δ of H^+-ATPases: at the interface between proton flow and ATP synthesis. *Biochim. Biophys. Acta* **1015** (1990) 379–390.
112. M. Müller, O. Pänke, W. Junge, S. Engelbrecht, F_1-ATPase: the C-terminal end of subunit γ is not required for ATP hydrolysis-driven rotation. *J. Biol. Chem*. **277** (2002) 23308–23313.
113. P.L. Sorgen, T.L. Caviston, R.C. Perry, B.D. Cain, Deletions in the second stalk of F_1F_0-ATP synthase in *Escherichia coli*. *J. Biol. Chem*. **273** (1998) 27873–27878.
114. P.L. Sorgen, M.R. Bubb, B.D. Cain, Lengthening the second stalk of F_1F_0 ATP synthase in Escherichia coli. *J. Biol. Chem*. **274** (1999) 36261–36266.
115. D.J. Cipriano, Y. Bi, S.D. Dunn, Genetic fusions of globular proteins to the epsilon subunit of the Escherichia coli ATP synthase: Implications for in vivo rotational catalysis and epsilon subunit function. *J. Biol. Chem*. **277** (2002) 16782–16790.
116. G. Kaim, P. Dimroth, Formation of a functionally active sodium-translocating hybrid F_1F_0 ATPase in *Propionigenium modestum* by homologous recombination. *Eur. J. Biochem*. **218** (1995) 937–944.
117. P.C. Jones, J. Hermolin, R.H. Fillingame, Mutations in single hairpin units of genetically fused subunit c provide support for a rotary catalytic mechanism in F_0F_1 ATP synthase. *J. Biol. Chem*. **275** (2000) 11355–11360.
118. D.A. Cherepanov, A. Mulkidjanian, W. Junge, Transient accumulation of elastic energy in proton translocating ATP synthase. *FEBS Lett*. **449** (1999) 1–6.
119. O. Pänke, B. Rumberg, Kinetic modeling of rotary CF_0F_1-ATP synthase: storage of elastic energy during energy transduction. *Biochim. Biophys. Acta* **1412** (1999) 118–128.
120. G. Drews, J.R. Golecki, Structure, molecular organization, and biosynthesis of membranes of purple bacteria; R.E. Blankenship, M.T. Madigan, C.E. Bauer, [2], in: *Advances in Photosynthesis: Anoxygenic Photosynthetic Bacteria* (1995) (Govindjee, ed), Kluwer, Dordrecht, pp. 231–257.
121. B. Rumberg, U. Becher, Multiple delta pH control of H^+-ATP synthase function in chloroplasts, in: *H^+-ATPase(ATP Synthase): Structure, Function, Biogenesis. The F_0F_1 Complex of Coupling Membranes* (1984) (S. Papa, K. Altendorf, L. Ernster, L. Packer, eds), Adriatica Editrice, Bari Italy, pp. 421–430.
122. D. Pogoryelor, J. Yu, T. Meier, J. Vonck, P. Dimroth, D.J. Müller, The C_{15}-ring of the *Spirulina platensis* F-ATP synthase: F_1/F_0 symmetry mismatch is not obligatory. *EMBO Rep*. **6**, 1040–1044.